3-1999

Radar Cross Section Enhancement of Simple Targets

Brian J. Crothers

AFIT/GE/ENG/99M-06

Radar Cross Section Enhancement

Of Simple Targets

THESIS
Brian J. Crothers
1Lt., USAF

AFIT/GE/ENG/99M-06

4

Approved for public release, distribution unlimited

AFIT/GE/ENG/99M-06

Radar Cross Section Enhancement of Simple Targets

THESIS

Presented to the Faculty of the Graduate School of Engineering

Of the Air Force Institute of Technology

In Partial Fulfillment of the

Requirements for the Degree of

Master of Science in Electrical Engineering

Brian J. Crothers

1Lt., USAF

March 1999

AFIT/GE/ENG/99M-06

Radar Cross Section Enhancement of Simple Targets

Brian J. Crothers
1Lt., USAF

Approved:

Chairman	date
Member	date
Member	date

ACKNOWLEDGEMENTS

I would like to thank my advisor, Dr. Vittal Pyati, for his support of my topic and advice during this effort. I would also like to thank Dr William Wood for sponsoring the effort as well as helpful suggestions on getting started with the research. I reserve a special thanks for Major Peter Collins who spent a great amount of time and energy helping me resolve many of my RCS range problems and data analysis issues. Also, I am grateful to Candi Emmans, who fabricated all the targets measured in this research. I would like to thank my classmates, especially Captain Bob Eigel and Captain Matt Craig for teaching me the basics of ACAD and FISC. I am forever indebted to my wife, Denise, who became a single parent of two children during much of this research, and still gave me unwavering support. Finally, I am grateful to God for giving the opportunity to study at AFIT and for his constant encouragement when situations seemed overwhelming.

Brian J Crothers

Table of Contents

Table of Figures

Abstract

This thesis explores the use of periodic open slots as passive antenna scatterers to enhance the radar cross section of a simple target. Two slot geometries are considered, thin rectangular slots and circular slots. Targets are modified with slot arrays of various element size, spacings, numbers, and geometries. These geometries were later backed by a cavity in an attempt to further enhance RCS. Measurements were taken and the results were compared to target baselines, which are nothing more than the unslotted version of the same target. Moment method solutions were also computed for comparisons with measured results. Additionally, an analytical expression for antenna scattering was tested as a means of achieving a fast first order accurate solution for target RCS.

It was found that the changes in RCS were generally consistent with the fields radiated by the slot array; small errors arise from slot coupling with edges and discontinuity scattering from the perpendicular component of the electric field. Cavity backed structures will provide additional levels of enhancements based on the incidence of illumination and cavity parameters. Moment method solutions are fairly accurate in their predictions of RCS, but extra care must be taken when modeling cavities. The analytic solution is shown to be reasonably accurate for aspects from 25^{o} above grazing incidence to broadside. Accuracy improves when the edge proximity is reduced. Results, in general, show that passive slot antenna arrays can be an effective tool for selective enhancement of a target's radar cross section.

CHAPTER 1: Introduction

In recent years, significant attention and research has been directed toward the reduction of radar cross section (RCS). RCS reduction represents a major portion of the Department of Defense tool kit of electronic combat techniques, but not all of it. The enhancement of radar cross section can also be an effective tool. Targets with enhanced cross section can be used to deceive and saturate threat radars. Enhancement devices can be concealed and used to mask true radar signatures from unwanted measuring sources. Targets passively enhanced can be tracked over greater ranges or greater aspects without sacrificing the payload and power costs to enhance the target actively (beaconing). If enhancement is applied over narrow regions it can be tracked for large distances at certain aspects while appearing as it normally would at all other incidences. This type of enhancement is useful for surveillance and intelligence gathering missions of remotely piloted vehicles (RPV's).

Radar cross section enhancement is defined as the augmentation of radar cross section above its normal value for a given aspect. Typically radar cross section enhancement is achieved by retroreflectors, such as a dihedral, trihedral, or spherical corner reflectors. Another example of a retroreflector is a Van Atta array. Retroreflectors are good for providing target enhancement over large spatial bandwidths. Their drawbacks are that they are visually obvious, making it less effective as a means of secretly masking true radar signatures. They may not be aerodynamically efficient, possibly limiting mission performance capabilities for air platforms. Finally, as stated above, some missions are better suited to narrow regions of enhancement both spatially and spectrally.

This thesis investigates the use of periodic slots as a passive augmentation system to enhance RCS on simple targets. The system is very similar to an antenna array except that the antennas behave purely as scatterers. Each slot radiates a scattered field in addition to the scattering centers on the baseline targets. By properly spacing the elements, the fields can be made to constructively add in preferred directions. Care must be taken, though, to ensure that the radiation pattern of the slot has a relatively strong radiated field in the direction of interest. In other words it makes little sense to try to enhance RCS in a null region of the radiation pattern for the slot. The field contributions of the slots in a monostatic sense can be expressed as

$$E^s = \sum_{1}^{N} E_i^s e^{-j2\mathbf{k}\bullet\mathbf{R}} \tag{1-1}$$

The two in the phase term accounts for the round trip distance of successive elements relative to the reference element. The normalized form of Equation (1-1) is simply the array factor for the equivalent antenna viewed monostaticly. Large backscatter return will occur for the array in regions where relative phase change between successive elements is $n\pi$ radians where n is an integer. The round trip separation then becomes $2n\pi$ and the coherent sum will be a maximum. Large backscatter from the array alone is not sufficient to enhance RCS. Radar cross section enhancement occurs when the total scattered field of the slot array also constructively adds with the fields scattered by the target's other scattering centers.

The enhanced scattering concept is drawn from techniques of reactive loading investigated in the fifties and sixties. Researchers then tried using the reactive nature of slots and other loads as a means of absorbing some of the incident energy and thus reducing the RCS. This technique, more generally referred to as impedance loading, was

largely abandoned as a reduction technique primarily due to bandwidth limitations of the loads. Also in situations where multiple loads were required, RCS was actually enhanced at some aspects within the frequency band where reduction was desired. It is the enhancement effect created by the multiple loads that is exploited. Researchers later favored exploring material absorber technology as a means of achieving broad band performance for the desired RCS reduction.

As implied above, the solution of the passive scattering problem is highly related to an antenna problem. The goal is to implement a passive antenna array on a target platform that scatters in such a way as to provide sufficient enhancement over specified target regions at specified frequency bands. Ideally, outside of either of these regions the slotted target signature is within an acceptable tolerance level of the baseline target from which it was derived. R. E Collin [4,5] developed a formulation whereby the scattered fields of an antenna could be characterized by two components: a structural mode scatterer and an antenna mode scatterer. The structural term represented the fields scattered by the antenna when the antenna terminal was short-circuited. The antenna mode term was the field radiated by the antenna itself in transmit mode. He modeled antenna scattering in terms of an S parameter matrix and was able to separate out the radiation contributions from the structural scattering contributions. The final result expressed the total scattered field of an antenna with a given load in terms of the scattering with a short circuit antenna (structural term) and a scaled value of the normalized radiated field of the antenna (antenna term). The equation is stated as:

$$E^s(Z_L) = E^s(0) - \left[\frac{I_0 Z_L}{I_a(Z_A + Z_L)}\right] E^r \tag{1-2}$$

E^s describes the scattered electric field; E^r describes the radiated field of the antenna in transmit mode; Z_L and Z_A describe the load and antenna impedance respectively; I_0 is the current on the shorted structure and I_a is the drive current on the antenna in the transmit mode.

Hansen [4] later generalized the formulation developed by Collin, as well as a similar formulation developed by Greene [3], so that either a matched or short circuit condition on the structural scatter could be used to describe the total scattered field from the antenna. He started by defining an antenna reflection coefficient as

$$\Gamma_A = \frac{Z_A - Z_L}{Z_A + Z_L} \tag{1-3}$$

Depending on whether a short circuit or matched load reference was used the total scattered field could be described as either

$$E^s(Z_L) = E^s(0) - \left[\frac{I_0(1-\Gamma_A)}{2I_a}\right]E^r \tag{1-4a}$$

Or

$$E^s(Z_L) = E^s(Z_A) + \left[\frac{I_m\Gamma_A}{I_a}\right]E^r \tag{1-4b}$$

Through some manipulations of Equation (1-4a) the scattering can be recast in terms of RCS as

$$\sigma = \left|\sqrt{\sigma_s} - (1-\Gamma_A)\sqrt{\sigma_A}e^{j\phi}\right|^2 \tag{1-5}$$

where the *s* subscript denotes the short circuit or structural component and the *a* subscript denotes the antenna component. The ϕ term is the relative phase between the structural and antenna scattered fields.

Equation (1-5) can be used to express the RCS of a slotted target in terms of the RCS of an unslotted target and a scaled value of the fields radiated by the slots themselves. For the target set in this research, the baseline (unslotted) targets represent structural mode or short circuit fields since the slots for these targets are essentially "shorted." The antenna or radiated mode term then becomes the field scattered by the slots independent of the surface contributions of the surrounding structure. The overall process of enhancement involves specifying the region and frequency band to be enhanced. From there, Equation (1-1) is used to determine the appropriate element spacing to enhance the region. Once this is determined, the result is converted to an RCS and applied as the antenna mode term in Equation (1-5). The baseline field serves as the structural term. The final result is an analytic expression of the total monostatic radar cross section.

The research effort is divided into three major parts. First RCS measurements of targets were made to observe that enhancement actually occurs. Second, comparisons of the measured results are made with predictions generated by computational electromagnetic codes (CEMs). Finally, both of these results are compared to the analytical expression of Equation (1-5) to make a qualitative assessment of how well the outlined approach works. Chapter Two of this thesis explores in detail the methodology used in performing target measurements. It also explains how targets were modeled to obtain the computational results, as well as the details involved with properly employing the approximate field summation equation. Chapter Three reports the results of measurements, computational predictions, and integrity of the analytical approximation. Finally, Chapter 4 summarizes conclusions and suggests follow-on research.

CHAPTER 2: METHODOLOGY

2.1 Experimentation

Experimentation was the major focus of this research. The actual targets were built and measured on the AFIT RCS range. The target set includes slotted flat plates (two sizes and two slot geometries), cavity backed plates, a spherical shell, and an ogive shell. For each measurement either the slot number, spacing, size, or combination was varied. The objective was to characterize enhanced scattering regions and magnitudes in terms of slot number, spacing, size, and geometry. Also of interest were the bandwidths of enhanced regions. Table 1 below shows the general test matrix used for all measurements.

Table2-1: General Test Matrix for Radar Cross Section Measurements

target	*frequency*	*freq step*	θ	ϕ	ϕ *step*	*pol*
Flat Plates Rectangular Slots (2 sizes)	(6.2- 18.2)GHz	+60 MHz	90^{o}	$(0\text{-}180)^{o}$	$+1^{o}$	VV HH
Flat Plates Circular Slots (2 sizes)	(6.2- 18.2)GHz	+60 MHz	90^{o}	$(0\text{-}180)^{o}$	$+1^{o}$	VV HH
Cavity Backed Plates Rectangular Slots (2 sizes)	(6.2- 18.2)GHz	+60 MHz	90^{o}	$(0\text{-}180)^{o}$	$+1^{o}$	VV HH
Cavity Backed Plates Circular Slots (2 sizes)	(6.2- 18.2)GHz	+60 MHz	90^{o}	$(0\text{-}180)^{o}$	$+1^{o}$	VV HH
Spherical Shell Rectangular Slots	(6.2- 18.2)GHz	+60 MHz	90^{o}	$(0\text{-}360)^{o}$	$+1^{o}$	VV HH
Ogive Shell Rectangular Slots	(6.2- 18.2)GHz	+60 MHz	90^{o}	$(0\text{-}180)^{o}$	$+1^{o}$	VV HH

The co-ordinate system is set up so that the grazing incidence of targets occur at $\phi=0^{o}$ and 180^{o}. Rectangularly slotted structures are aligned with the long dimension of the slots parallel to the *z*-axis, except for the ogive, whose long dimension is parallel with the *x-axis*. Vertically polarized fields are *z* directed and horizontally polarized fields are y directed. A diagram of the target setup and coordinates is shown in Figure 2.1 below.

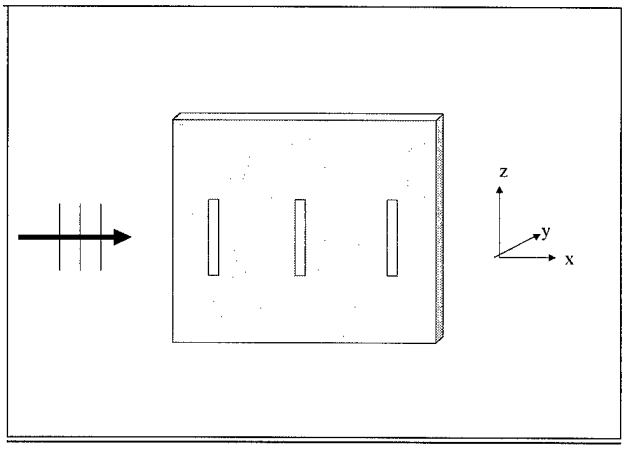

Figure2. 1: Target setup and coordinate system

2.1.1 Flat Plates and Cavity Backed Plates

Four square aluminum plates were fabricated for measurements: two were designed to be three wavelengths long at 10GHz, and the other two designed to be three wavelengths long at 15GHZ. Each plate was loaded with either five rectangular slots 1λ long spaced .5λ apart or with nine circular slots spaced .75λ apart in a 3X3 array where the radius was defined by the length required to make it fundamentally resonant at the reference frequency. Element number and spacing was changed by using aluminum tape to short out undesired elements. For rectangular slots the tape could also be used to

reduce the length of the slot by shorting out parts of the original slots. For example, the slots could be made .5λ by shorting the top and bottom quarters of the original slot.

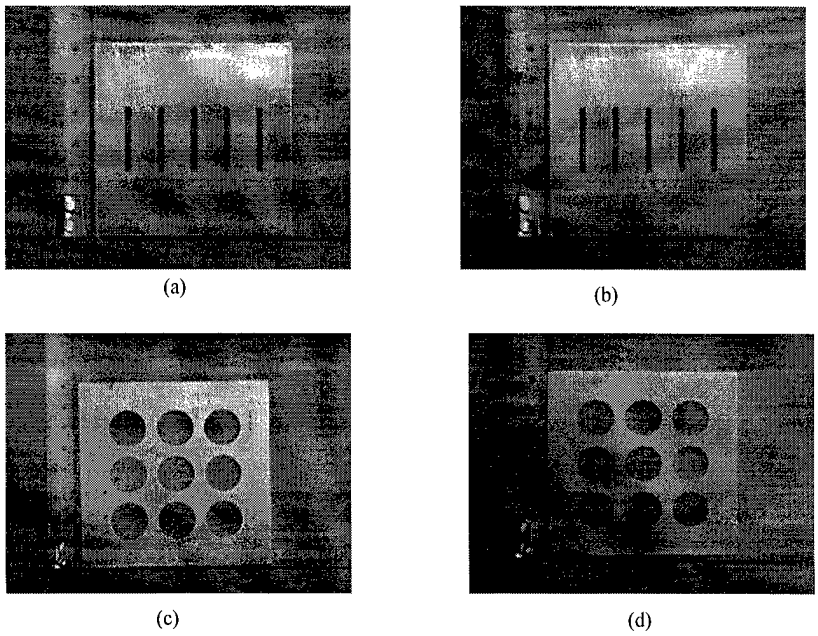

Figure2. 2: (a) Large rectangular slotted plate. (b) Small rectangular slotted plate. (c) Large circularly slotted plate. (d) Small circularly slotted plate

Intuitively, the introduction of the tape could induce errors in measurement. A short experiment was conducted where the tape was placed randomly on several different plate targets, and RCS measurements were taken. The results were compared to measurements taken of the same targets without the tape. In all cases there was virtually no change in the measured RCS of the targets.

Both rectangular and circular slot targets were measured primarily to investigate the dependence of target enhancement with respect to polarization. Rectangular slots can be approximated by a thin magnetic dipole. Dipoles, in general, are very polarization

sensitive, radiating efficiently only when excited by the appropriate field in its long dimension. The rectangular slot excited along the short dimension appears essentially as a flat plate. The circular slot, however, is very polarization insensitive. This is primarily because the slot itself appears the same regardless of the orientation of the incident electric field. This does not mean, though, that the target RCS will be the same for all polarizations. Most targets will have some other scattering mechanism that is polarization dependant, such as traveling wave or creeping wave diffraction for perpendicular polarization. Also of importance regarding geometries is the strength of the fields scattered by the slots. It can be proven that for the fundamental resonant mode in the far field, the circular slot scatters a larger field compared to a thin rectangular slot or the limiting case of a square slot. The disadvantage though is that a resonant circular slot requires more area than either a resonant rectangular or square slot.

The cavity backings were designed to fit behind either the large or small plates and add a 1λ depth dimension to the target at the reference frequency. They were fastened to the plate using aluminum tape to connect the outside edges. Figure2.3 shows pictures of the cavities and how they attach to the plate. The cavity backing serves to redirect energy back into the backscatter direction, providing an additional enhancement factor. Depending on the incident angle and cavity depth, the energy will undergo a number of bounces and is eventually reradiated out. The incidence angle and cavity depth determine the total path length, and thus the relative phase of the field, which in turn affects the overall level of enhancement achieved. Cavity analysis details are provided in Chapter 3.

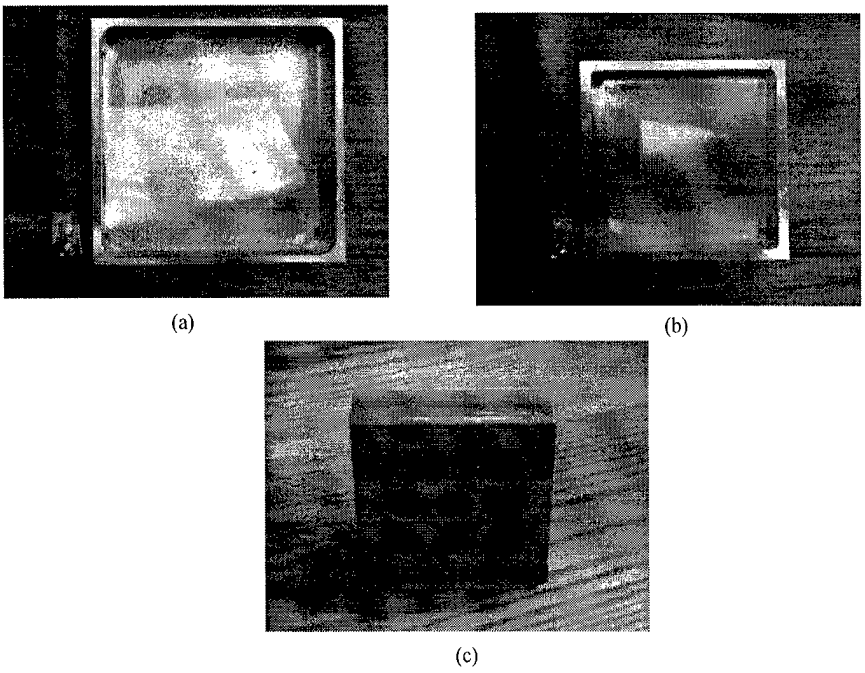

Figure2. 3: (a) Large cavity backing (b) Small cavity backing (c) Plate mounted on cavity backing.

2.1.2 Sphere and Ogive Shells

Sphere fabrication paralleled that of the flat plates in the sense that sphere diameter was defined by the 3λ length referenced at 10 and 15GHz. They were modified by five rectangular slots in the same manner as on the flat plates; however, the lengths were referenced radially, not linearly as with the flat plate. In other words the λ/2 separation between elements and the λ slot length are arc lengths rather than a straight distance. Like the plate, the slots of the sphere are oriented in the *z* direction.

Ogive construction was piecewise. That is, the ends of the ogive were rounded off with a constant curvature rather than the sharp tip normally associated with an ogive. This was done primarily as a fabrication convenience but also has some merit considering

that a curved surface can be considered an RCS enhancement device for a tip scatterer. The generating chord of the ogive was 4λ, again with respect to the 10 and 15GHz reference. The center width of the ogive was constructed to be 2λ long. Only three slots were cut on the ogive but they maintained the λ/2 radial separation of their spherical counterparts. The slots of the ogive were aligned along the long dimension of the target, i.e. the *x* direction rather the *z* direction as in all previous cases. Pictures of the sphere and ogive targets are shown below (Figure 2.4).

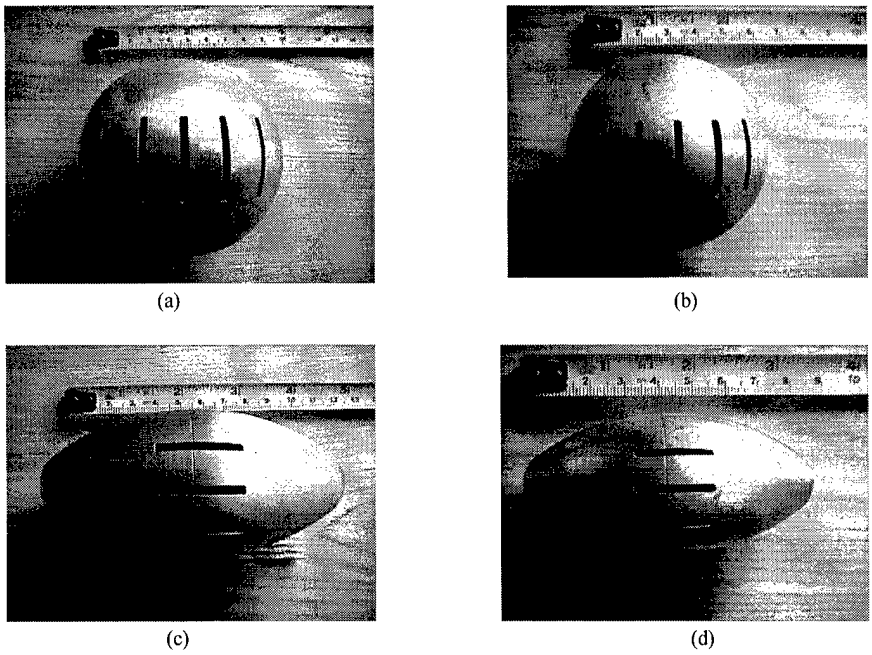

Figure2.4:Spheres and Ogives (a) large sphere (b) small sphere (c) large ogive (d) small ogive

The motivation for measuring sphere and ogive targets is to explore the effects of different cavity back geometries. Less emphasis is placed on these other geometries though. This is primarily because it is a much more difficult problem to try to calculate, let alone attempt to control, the cavity response. Measurements, though, will give some

insight as to whether or not it may be significantly beneficial to explore in greater detail these other geometries.

2.2 Computational Methods

Unlike the simple targets investigated here, full-scale operational targets are not easy or relatively cheap to build. Likewise, they can be equally costly and complicated when it comes to measuring full-scale targets. While measured data on real targets gives us the best picture of how a system will behave this is not always practical. It is often necessary to rely on computational methods to get a good sense of the system's actual behavior. Computational methods, though, are only as good as the accuracy of the true RCS they can predict. High frequency codes such as XPATCH, a Physical Optics \Physical Theory of Diffraction based code, yield good results when the target size is very large relative to a wavelength. Scattering can be treated as a localized phenomenon at the scattering centers, and the total scattered field is merely the coherent sum of all the scattering centers. When target sizes are smaller, low frequency codes such as the method of moments generally provide more accurate results. Low frequency codes generally apply exact equations, incorporating Maxwell's equations, boundary conditions, and equivalence principles to calculate scattering currents or scattered fields. High frequency codes generally use an asymptotic approximation of the true scattering phenomena. In general it is expected that techniques incorporating exact methods yield more accurate results. FISC (Fast Illinois Solver Code), a moment method code, was used to generate RCS predictions of the targets. The RCS data was compared against measured results to assess the level of accuracy between measured and computational results.

FISC was developed by the University of Illinois Center for Computational Electromagnetic and DEMACO. It calculates radar cross section of targets using the method of moments technique. The code is available along with the XPATCH v2.4 suite. The code accepts triangular facet files as the input target files. The matrix equation is solved by the conjugate gradient method. FISC's computational power comes from the implementation of the multilevel fast multipole algorithm (MLFMA). The MLFMA reduces the CPU and memory requirements from an order of N^2 to an order of NlogN where N is the number of unknowns.

Inputs for FISC were facet files generated in ACAD v9.0. The CIFER utility available on the XPATCH GUI then converts ACAD facet files to DEMACO facet files usable by both XPATCH and FISC. The facet file was triangularly meshed and scaled so that edge lengths did not exceed .1λ. The .1λ facet edge length is the generally accepted length required for sufficient accuracy in moment method codes. FISC will internally remesh the target for a given frequency if the original input file does not meet the edge length criteria for the given accuracy level. The criterion is .2λ for low accuracy calculations and .1λ for high accuracy. Certain geometries, though, may require finer meshing to achieve accurate results. This was the case for targets loaded with circular slots. Facet files approximate circles as an N segmented equilateral polygon. In order to better capture the affects of circular geometry the slot segmentation should be sufficiently high; segment lengths around .05λ appear to be sufficient. Figure 2.5 below shows a facet file of a flat plate loaded with circular slots. Finer meshing does, however, increase the number of unknowns, adding larger memory requirements and CPU time to calculate the RCS.

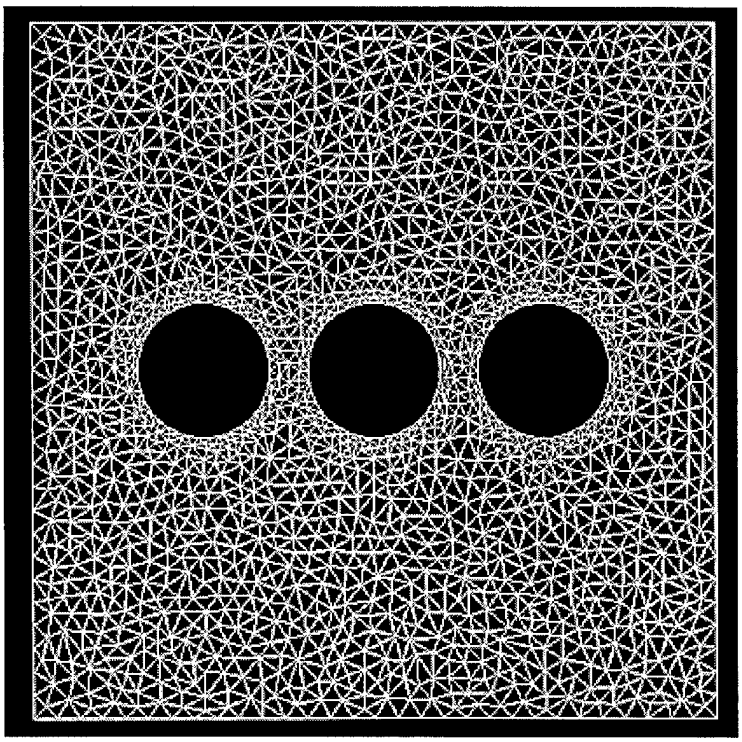

Figure2. 5: Facet file of plate target with circular slots.

2.3 Analytical Approach

The analytical expression of the radar cross section of Equation (1-5) provides us with information of what the radiated component of scattering must be to achieve a desired RCS enhancement. As in the case of CEM solutions, the analytical approximation is only as good as its ability to approach the true solution. The one major flaw in using the results of Equation (1-5) is that it treats only scattering contributions from the baseline or antenna independent of the other. Interactions between the target surface and the slots must also be considered if the solution is to be highly accurate. The most prominent interaction to be considered is the slot-edge coupling and discontinuity scattering from the perpendicular component of the incident E-field. The discontinuity scatterers will add in the same manner as the radiated fields of the array, although its relative phase will not necessarily be the same. Thus, the true RCS may vary significantly

in some regions if there is large constructive or destructive interference with the dominant scatterers. The effect is more pronounced as the incidence angle creates a larger perpendicular component of the illuminating E-field.

The purpose of using Equation (1-5), though, is to get a first order sense of the system's behavior. It can still be a useful tool if its predicted RCS in the region of interest is sufficiently accurate and the prediction captures the general phenomenology of the total scattering, that is, if the RCS pattern of the analytical expression closely follows the trends of the true signature, it still gives good insight into the target behavior --even though magnitudes may be off. Investigating how much confidence can be placed on the analytical approximations was the final objective in this thesis research.

The major hurdle that must be overcome for the analysis to work is establishing proper phase references. For example, if short circuit RCS data is collected from a range the phase reference is typically near the radar. If the data was collected from a CEM code, where the source is located at infinity, the reference is typically in some target plane. In either case the phase reference for the array of the loaded structure would be at the center element of the array. In order to properly add the fields a common phase reference must be established. Thus properly implementing the scattered field equations requires some knowledge of how the components are phase referenced.

Measured RCS and phase data were used for the baseline values. The reference, therefore is at the radar. The most convenient reference point for the baseline would be the target center because there, it is collocated with the phase reference of the array as well as being a stationary point on the target as it rotates. Once the reference was established, the phase return of the baseline target needed to be adjusted so that its

reference was relative to the target center itself rather than the radar. This is accomplished by subtracting the phase of the return at each angle of incidence by the phase return at broadside incidence. At broadside incidence the target is uniformly illuminated, which means complex addition of the scattered fields does not alter the phase relative to the individual terms. Because there is no phase change induced on the total scattered field relative to the addition of the individual scattered fields, the broadside-incident phase essentially tracks the distance from the radar to the target center. Subtracting out that distance (phase) at all incident angles creates a new phase reference relative to the target center. Once the baseline and array have the same reference point, the fields can be coherently added.

Next, radiated fields of the slots themselves must be calculated. Before the fields are calculated a few simplifying assumptions are made. First, field patterns are calculated assuming uniform illumination across the slot rather than the modal field. Second the illumination is uniform at all incidences; that is, no phase tapering is considered from off normal incidence. Finally, all fields scattered from the target surface and thus their equivalent currents are assumed to be accounted for in the structural term of Equation (1-5). The slots then see a PEC surface with no currents on it. The surface, because it does not contribute anything to slots scattering, can be extended infinitely without perturbing the fields. The scattering problem is now equivalent to the radiation problem of an aperture mounted on an infinite ground plane. The fields are calculated by first finding the equivalent magnetic surface current.

$$\mathbf{M}_s = -2\hat{\mathbf{n}} \times \mathbf{E} \tag{2-1}$$

Once the currents are known they can be plugged into the radiation integral to determine the fields. Using the target layout and coordinate system of Figure2.1 and recalling that the scan plane is $\theta=90^{\circ}$ the radiated fields can be expressed as:

(2-2) $$E_{\phi} = \frac{jkabM_s}{4\pi r}\frac{\sin(X_1)}{X_1}e^{-jkr}$$ Rectangular Slots Hpol

(2-3) $$E_{\phi} = \frac{jka^2 M_s}{2r}\frac{J_1(X_2)}{X_2}e^{-jkr}$$ Circular Slots Hpol

(2-4) $$E_{\theta} = \frac{jka^2 M_s}{2r}\frac{J_1(X_2)}{X_2}\cos(\phi)e^{-jkr}$$ Circular Slots Vpol

where;

$$X_1 = \frac{kb\cos\phi}{2}$$

$$X_2 = ka\cos\phi$$

Recall that rectangular slots are not strongly excited in the vertical polarization therefore they will not radiate significant fields. This will be discussed in Chapter 3 with greater detail.

Although this thesis research is dominantly experimental, the incorporation of computational and analytic techniques serve as excellent validation methods of experimental results; as well as providing some insight in to the general scattering behavior of the targets.

CHAPTER 3: RESULTS AND ANALYSIS

3.1: Square Plate Rectangular Slots

Analysis starts by examining the large square plate configured with three slots λ/2 long and spaced 1λ apart. First, the effects of polarization are examined. As stated in Chapter 2, thin rectangular slots are analogous to a magnetic dipole. In the horizontal polarization the magnetic field will be parallel to the long dimension of the slot and thus the antenna is strongly excited and radiates significant fields into space. In the case of vertical polarization, however, the magnetic field is parallel to the short dimension of the slot. Dipoles do not radiate efficiently when excited with cross polarized fields, and thus little affect on the target signature compared to its baseline is expected. The baseline is considered to be an unslotted version of the target under test. Figure 3.1 and Figure3.2 show plots of the target RCS vs. the baseline at 10.04GHz for the two polarizations.

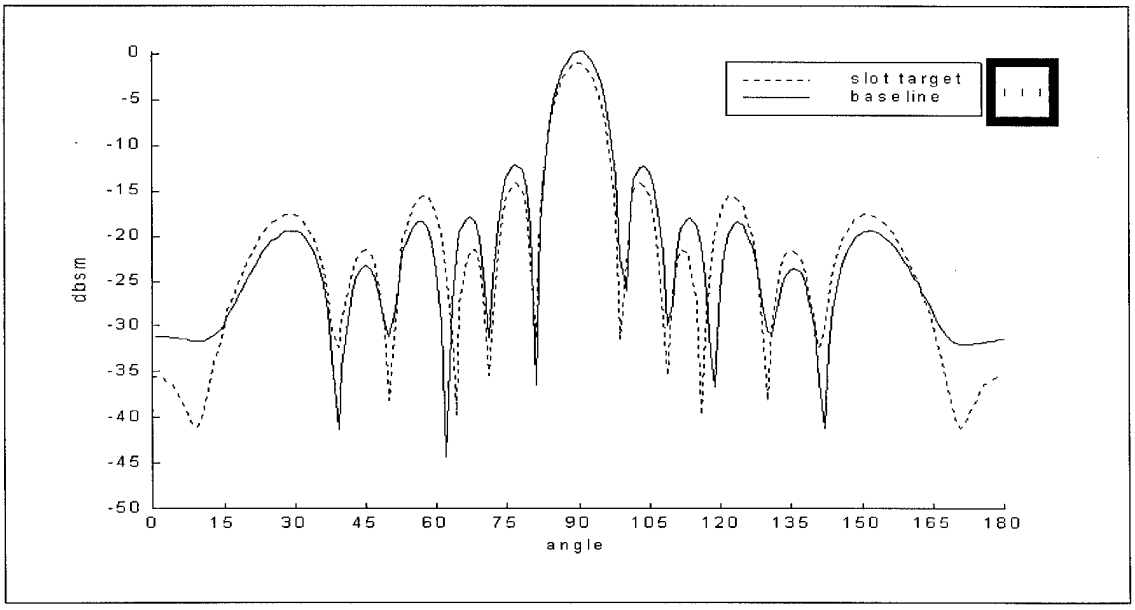

Figure 3. 1: Large plate 3 Slots (d = λ) at 10.04GHz Hpol

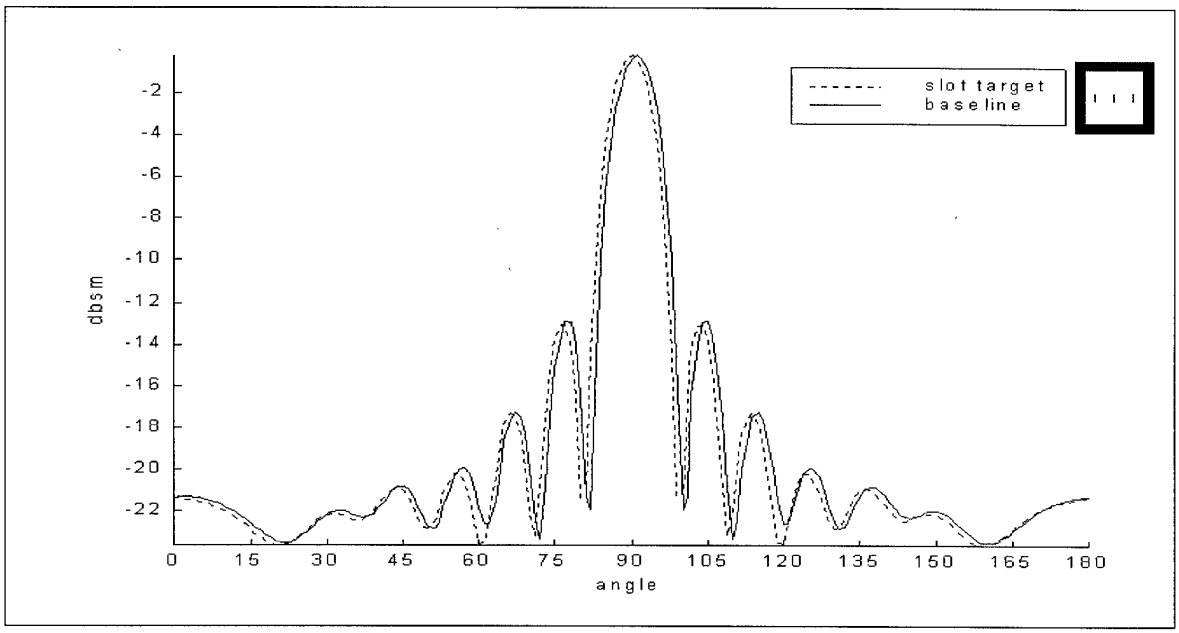

Figure 3. 2: Large Plate 3 Slots (d = λ) at 10.04GHz Vpol

It is very apparent that the slots have little effect in the cross-polarized case. Another way to approach the problem is to treat the slot or aperture as a very small waveguide since in practice there is a finite dimension of slot thickness. For the horizontal polarization the incident field frequency is slightly greater than that of the cutoff frequency for the guide. The wavenumber is real and therefore the wave suffers no attenuation as it propagates into the aperture. In the short dimension the incident frequency is far below the cut off for the guide, in fact it is approximately ten times lower than that of the guide. The wavenumber for the guide becomes imaginary and can be expressed as

$$k_g = -jk\sqrt{\left(\frac{f_c}{f}\right)^2 - 1} \tag{3-1}$$

The imaginary wave number at the interface of the aperture indicates attenuation. For a 10GHz vertically polarized incident field the attenuation constant is about e^{-2083x}.

The incident field is reduced more than two orders of magnitude within $\lambda/100$ thickness. The fields reradiated are thus very small and do not significantly affect the total target signature.

From Equation (1-5) it is hypothesizes that the changes in RCS are due primarily to the fields radiated by the slots themselves. One way to test this is to perform a vectoral background subtraction of the baseline target from the slotted target. The resultant difference, theoretically, is the radiated fields of the array plus, of course, the interactions of the slots with the scattering mechanisms of baseline target. Getting an accurate background subtraction for the targets is extremely difficult, unfortunately. The target must be removed after either a baseline or target measurement to remove or add conductive tape for the next target measurement. When the target is remounted in a later measurement, a slight misalignment of that target with respect to the former will destroy much of the phase information essential for an accurate background subtraction. Techniques similar to the method described in Chapter 2 used to establish a phase reference for the analytical solution could be employed here to try to minimize the information lost due to phase errors. The final result, though not entirely accurate, is sufficient enough to at least demonstrate that the difference fields are a product of the monostatic array factor. Figure 3.3 below shows how the vectoral difference compares to the monostatic array factor for the three slot large plate mentioned above. Note particularly how well the nulls of the difference plot align with the array factor nulls and that the relative peaks of the lobes align fairly well with the array factor lobe peaks.

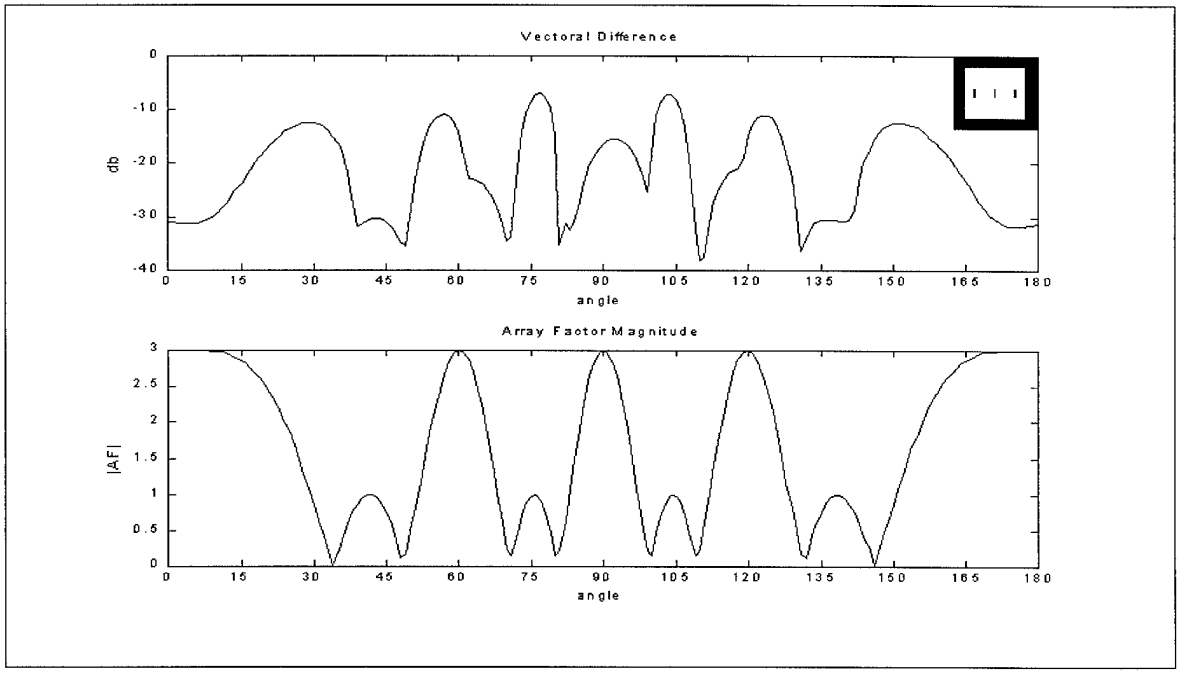

Figure 3. 3: Background subtraction of large 3slot plate (d = l) with target baseline. The plot above illustrates the hypothesis that RCS changes are primarily accounted for from the array fields .

Next, it is desirable to observe how the signature changes as the number and spacing of the slots change. Three cases are considered; first the target of Figure3.1, that same target with element spacing changed from λ to $\lambda/2$ (Figure3.4a), and finally the target with two more elements added keeping the $\lambda/2$ spacing (Figure3.4b).

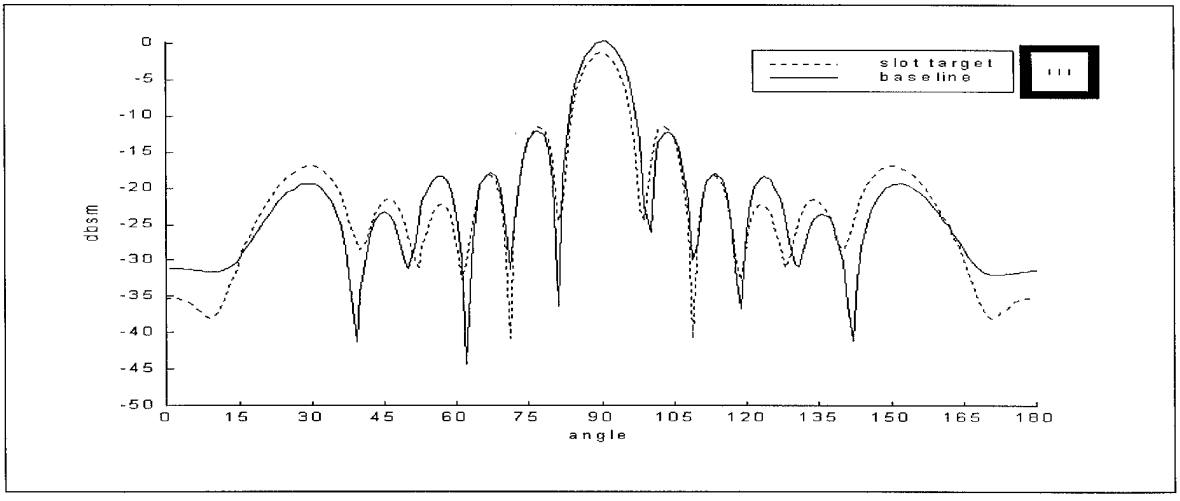

Figure 3. 4a: Large 3 Slot Plate (d = $\lambda/2$) at 10.04GHz Hpol

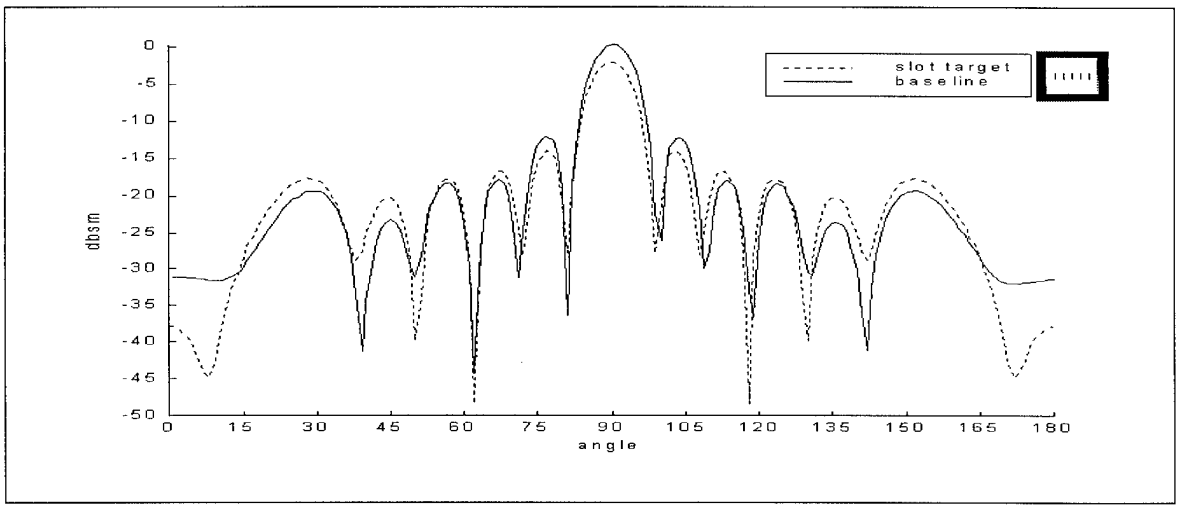

Fig3.4b: Large 5 Slot Plate (d = λ/2) at 10.04GHz Hpol

Because of symmetry about the broadside axis of both baseline and slotted targets only phenomena from 0 ° to 90 ° will be referenced. One feature common to all three cases is signature enhancement in the region of 15 ° to 45 °. There is enhancement in these regions regardless of whether the monostatic array factor of Equation (1-1) predicts it or not. The enhanced scattering in this region is most likely due to the discontinuity scattering of the perpendicular component of the incident E-field for the horizontal polarization. From grazing to 45° it is greater than or equal to the parallel component thus we would expect that feature to be more significant. From broadside to 45° the perpendicular component is not as significant so most enhanced scattering is presumably the effect of the slot array.

Enhancement by the array of the targets in Figure 3.1 and Figures 3.4 is what is of particular interest though. There are three sidelobe peaks at approximately 56°, 67° and 76° where enhancement effects can be considered to come purely from the array. For the case of three slots with λ separation the lobe at 56° is significantly enhanced while the lobes at 67° and 75° are significantly reduced. If this phenomenology is compared to the

monostatic array factor for the given array configuration, Figure 3.5, it is it seen that the 75^{o} lobe occurs near were the array factor has its maximum negative value. This is a reasonable explanation for the reduction in this region. The 67^{o} lobe falls in the null of the array suggesting no further enhancement or reduction effects. The reductions in this area is likely due to coupling effects with the edges. This claim can be loosely substantiated by comparison with the target of Figure 3.4a. The slots of the target of Figure 3.4a are further removed from the plate edges. The monostatic array factor for this case (Figure3.6) also has a null in the region about 67^{o}. In this case though the slot target RCS is virtually the same as the baseline. The only remaining difference between this target and that of Figure3.1 then is the edge proximity.

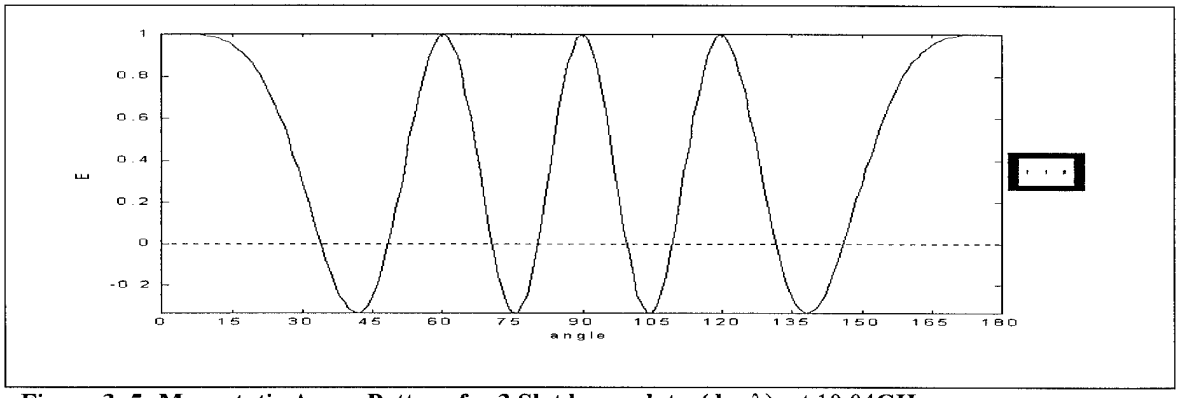

Figure 3. 5 :Monostatic Array Pattern for 3 Slot large plate (d = λ) at 10.04GHz

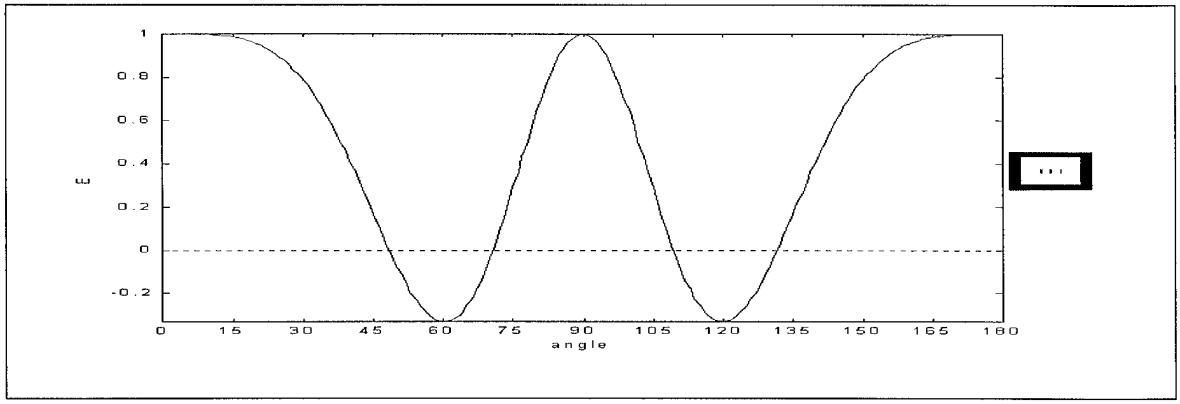

Figure 3. 6: Monostatic Array Pattern for 3 Slot large plate (d = λ/2) at 10.04GHz

Next, consider the remaining peaks of the target of Figure3.4a. The lobe at 57 ^{o} is reduced and the other two lobes are relatively unaffected, showing only minimal changes relative to the baseline. Comparing these observations with the array factor, there is again some good correspondence. The array factor magnitude in both cases is about .2 indicating not much is to be expected in these regions

Finally, consider the effect of increasing the slot number to five while maintaining the $\lambda/2$ spacing (Figure 3.4b). RCS is enhanced at the 56 ^{o} lobe and 67 ^{o} lobe and slightly reduced at 75 ^{o}. Comparing these attributes to the associated array factor (Figure3.7) it is seen there is minor positive constructive adding in the array factor at 56^{o} ad 67^{o}; there is probably some higher order effects giving it some boost as well, such as a stronger interelement or edge coupling effect. The array factor is at a negative maxima near 75^{o} were the RCS of the target is significantly reduced indicating probable cancellation effects.

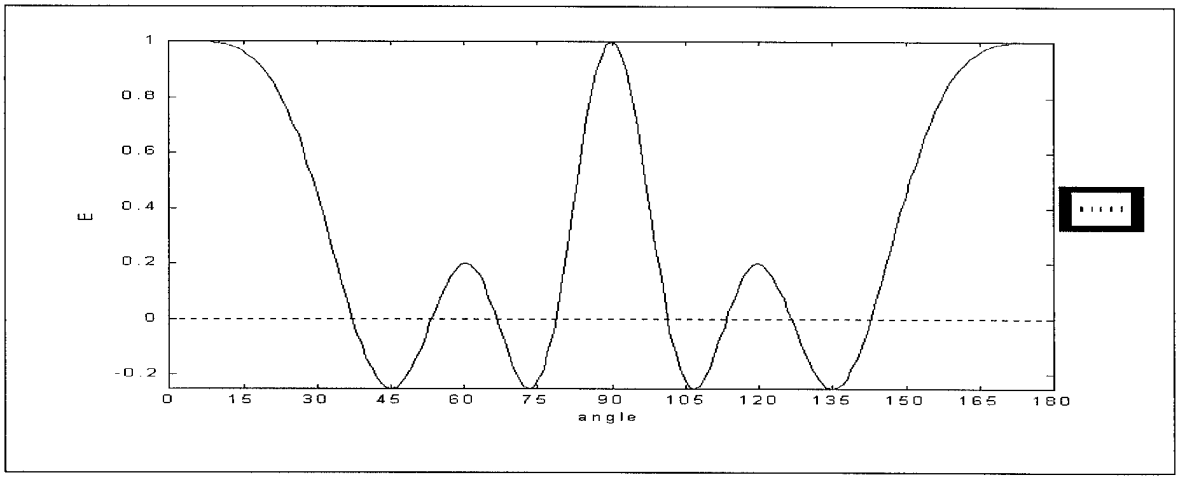

Figure 3. 7: Monostatic Array Pattern 5 Slots (d = $\lambda/2$) at 10.04 GHz

Slot size is also an important consideration in the enhancement of RCS. Electrical size of the slot determines the radiation pattern, and to some extent radiation efficiency.

Changes in pattern or efficiency in the slots will affect the over enhancement for a particular region. For example, consider the small square plate with three slots and λ spacing illuminated at 15.02 GHz, with a slot length of λ (Figure3.8a) and then with a slot length of $\lambda/2$ (Figure3.8b). The slots are second mode resonant for the case when the length is λ, but all other target parameters remain the same as that of Figure3.8b which has fundamentally resonant slots. The actual field distribution for the second mode is sinusoidal inside the aperture compared to the cosinusoidal distribution of the first mode. The sinusoidal distribution puts a null at broadside and has a maximum near the endfire direction. Thus, second mode resonance in the $\theta=90^{o}$ scan plane contributes no radiated component in the backscatter direction so no enhancement would be anticipated. Figure 3.9 shows the RCS pattern for the plate when slots are in first and second resonant mode.

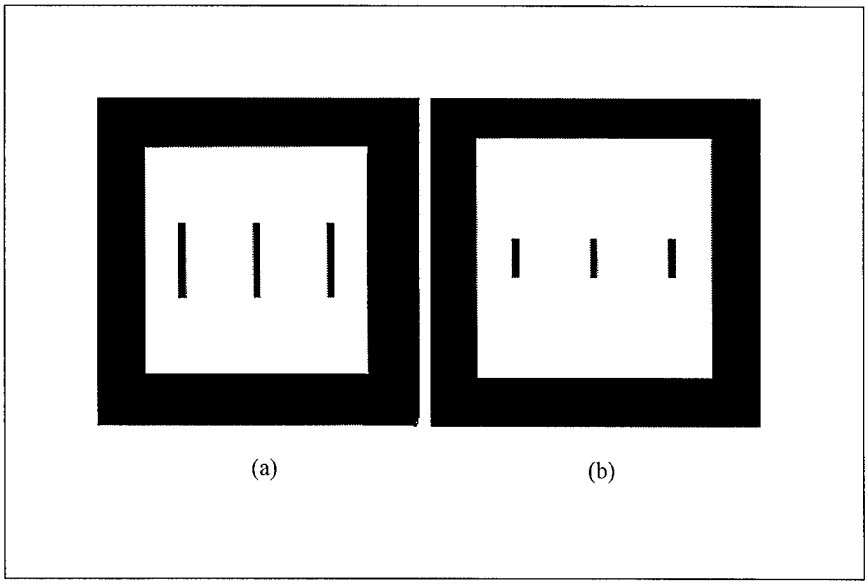

Figure 3. 8: Small 3 slot plates (d =λ) [a] 1-λ slot length resonates in second mode [b] $\lambda/2$ slot length resonates in fundamental mode

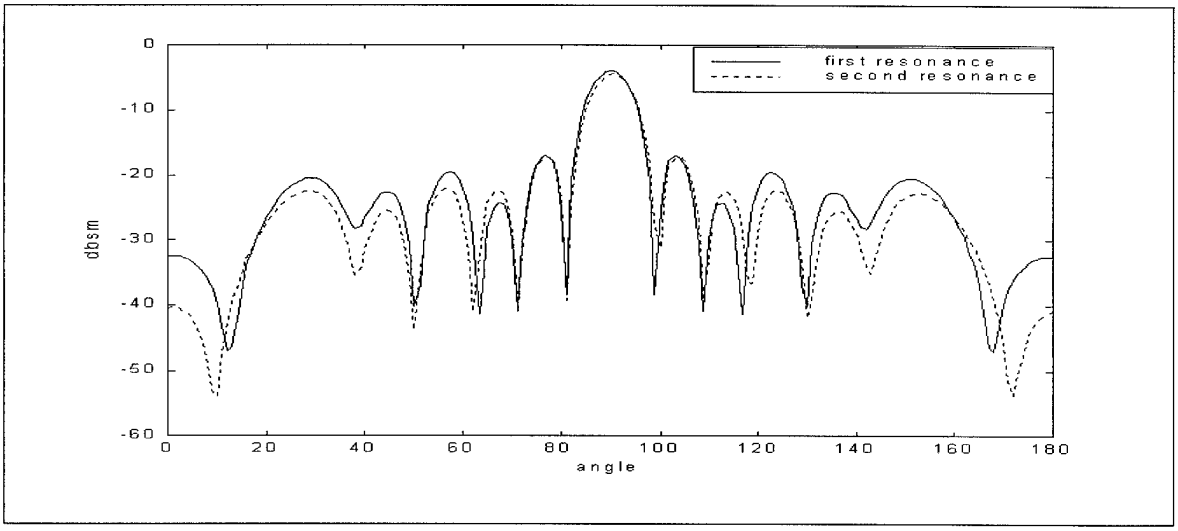

Figure 3. 9: small 3 slot plate (d = λ) at 15.02GHz Hpol for first and second resonance

In third mode resonance the distribution is cosinusoidal again, however the relative increase in electrical size introduces sidelobes in the pattern, thus not all the energy is available in the main beam. This will detract from enhancement as well, for the most part. Generally speaking, the best enhancement performance occurs at first resonance for plate structures. It will be demonstrated later that cavity structures are not as limited in this regard.

It was mentioned earlier that below the first resonance (cutoff) the field is attenuated at the aperture. The vanishing field is analogous in concept to a short circuit. That is, the further away from resonance the more the target appears as the baseline. To illustrate this, consider the small plate of Figure3.8b, where the resonance is 15GHz, illuminated near the large plate's slot resonance (10.04GHz). The incident field is approximately 5GHz below the cutoff of the slot and is attenuated as roughly e^{-353x}. The field is significantly reduced but has not quite vanished. There is still possibility for minor differences in RCS, but the slotted target signature starts to approach the unslotted

(baseline) signature. The small plate RCS is plotted in Figure 3.10 below. If the incident frequency is reduced even further, to 7.52GHz, the attenuation is stronger in the slots and the slotted target appears virtually the same as the baseline target.

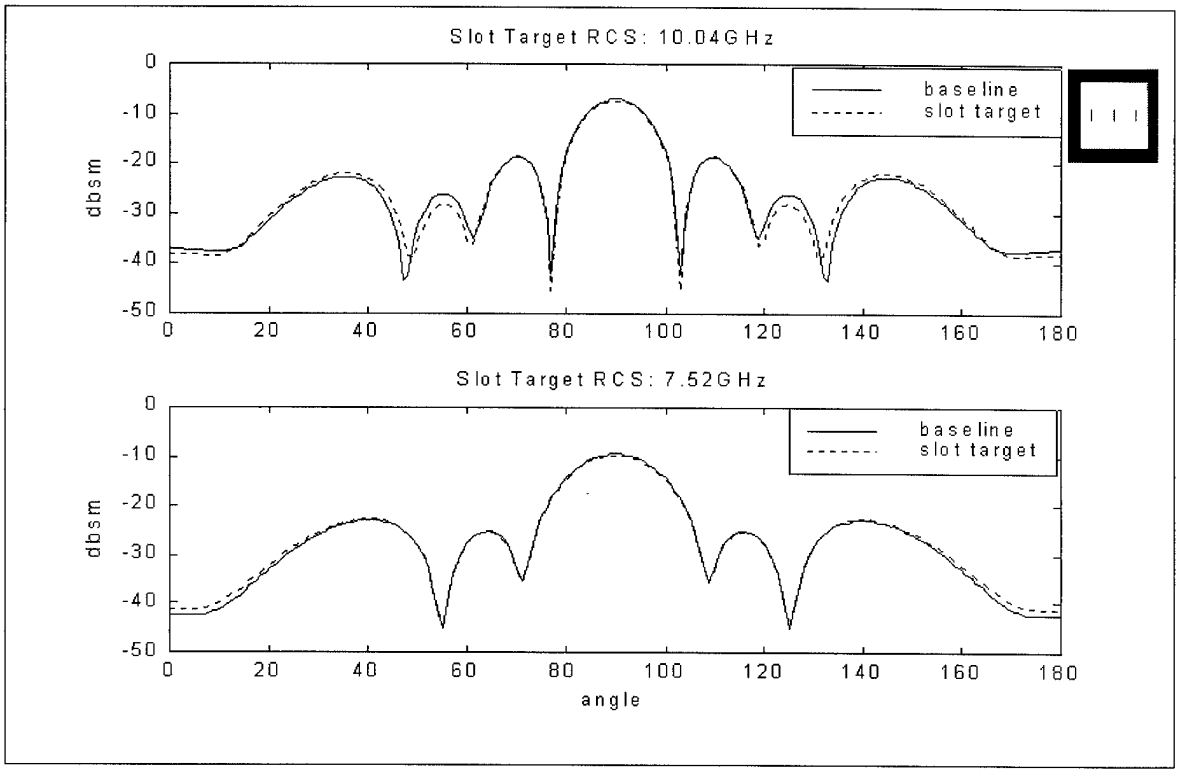

Figure 3. 10: Small 3 slot plate (d = λ) at 10.04GHz and 7.52GHz Hpol

Next, numerical and analytical results must be compared with the measured data to assess the accuracy with which they can predict measured data. The initial case of the large plate with three slots and λ separation is taken as an example. First, measured results are compared with the analytical solution near the resonant frequency. Again the accuracy of the analytic approximation is of importance because it can give quick insight into the enhanced zones and their magnitudes before expending valuable computer resources on a numerical solution. The analytic approximation is compared against the measured data for the horizontal polarization at 10.04GHz in Figure 3.11 below. For all

but the second and fourth sidelobe maximums the analytical results are within a 1dB error of the measured RCS at sidelobe peaks. The maximum error is about 4dB at the second sidelobe peak. Near grazing incidences are not very good though. This is because near grazing incidence there are many significant second order effects not accounted for in the expression. Particularly, the strong edge coupling of radiated fields and the break down of the assumption made about no phase tapering. The beam alone can be fairly significant putting the true fields somewhere other than at the grazing incidences. This trend near grazing appears in all analytical calculations for both polarizations. The analytical results for most cases are good, though, from about 25° to 90° for both polarizations and both rectangular and circular slot geometries (Circular slots are treated later).

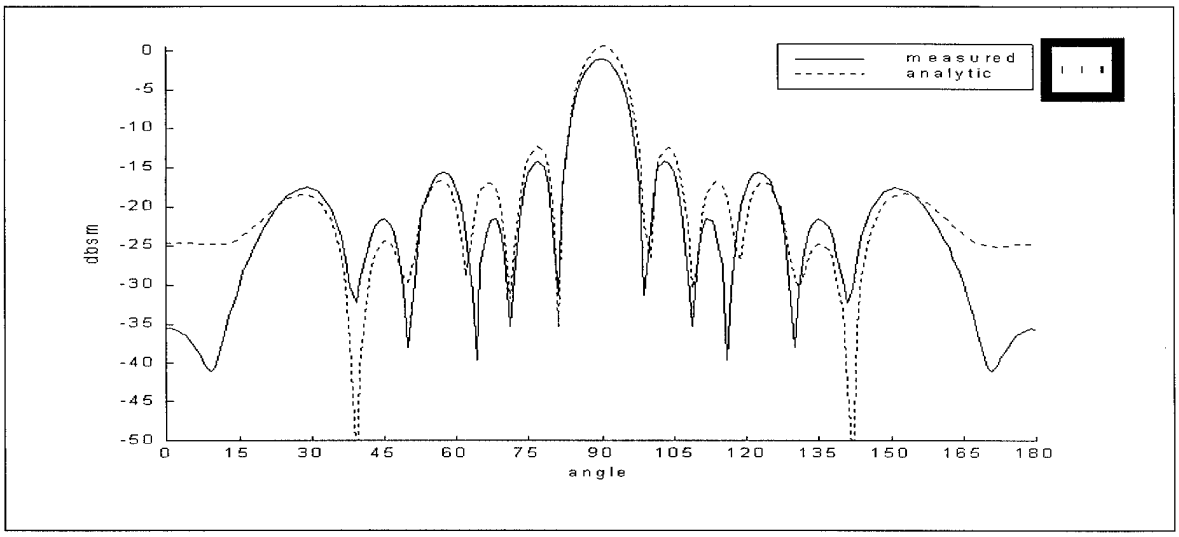

Figure 3. 11: Measured RCS vs. Analytic Prediction for large 3slot plate (d = λ) at 10.04 GHz Hpol

For the vertically polarized case with rectangular slots the fields in the aperture is wiped out almost immediately due to the high attenuation constant associated with the first vertical mode. The analytic solution will be essentially the same as the baseline.

Finally, the more rigorous method of moments solution from FISC is assessed. Figure 3.12 below plots the numerical solution and measured results for both polarizations at 10.04GHz incident frequency. The horizontal solution converges much better to the measured RCS than its vertical counterpart. The vertical case was meshed three times finer than the .1λ edge standard with no further improvement than the standard mesh. However, from the actual measured data compared to the baseline it can be seen that no enhancement is achieved for the cross polarized case. For the horizontal polarization, errors compared with the measured results occur in the same region as they appeared for the analytical solution though not as severe. The largest error is about 3dB at the second and fourth sidelobe.

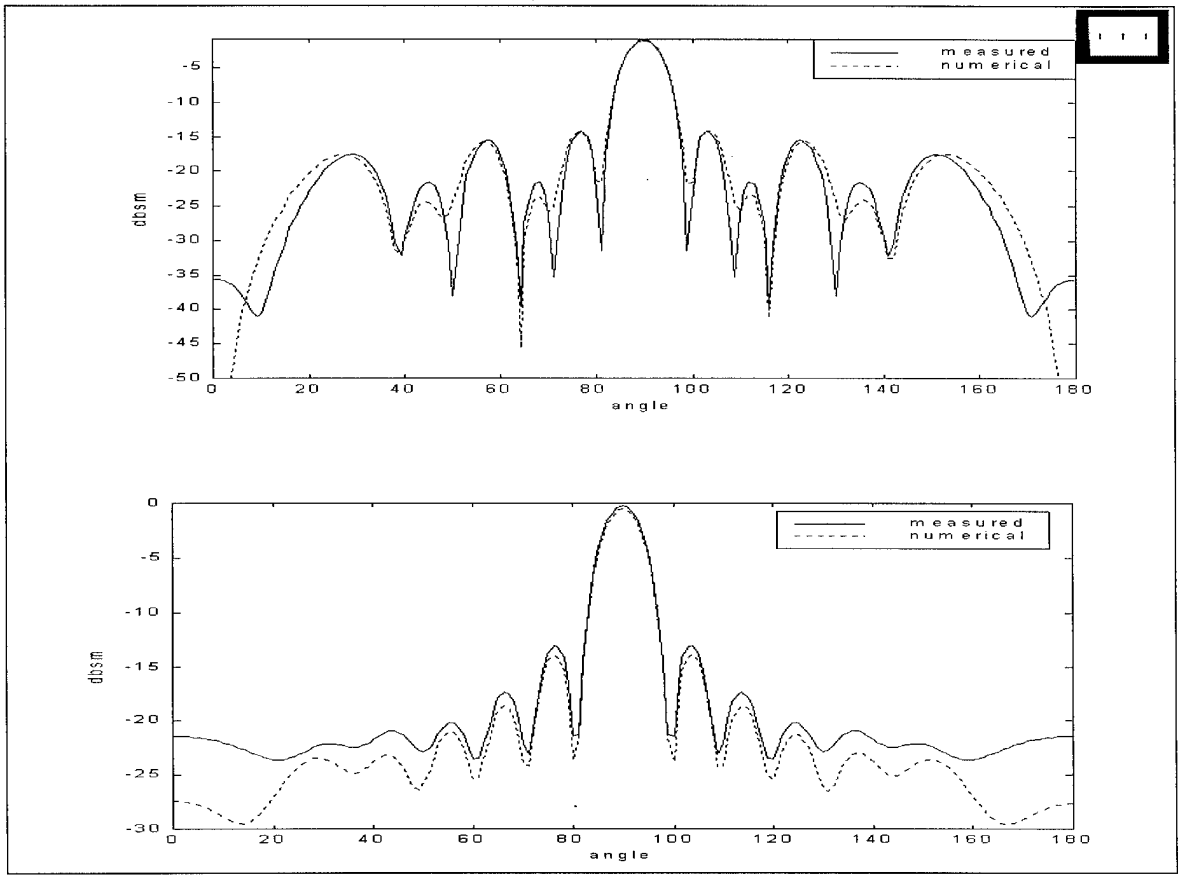

Figure 3. 12: Measured RCS vs. MoM Prediction for Large Plate 3Slot (d = λ) at 10.04 GHz Top: Hpol Bottom: Vpol

3. 2: Square Plates Circular Slots

The next target type investigated is the square plate with circular slots. The primary motivation for enhancement using circular slots is that the slots are theoretically insensitive to polarization. In practice this means the incident field will not suffer any attenuation as it makes contact with the freespace-aperture interface as it did in the case of the thin rectangular slot when the field was cross polarized. Analysis begins by examining the large square plate with two circular slots spaced 1.5λ apart. Figure 3.13 plots the RCS for both horizontal and vertical polarizations for a frequency of 10.04 GHz. For both cases the enhanced regions occur is the same vicinity, though, the levels are different for the two polarizations. The major differences are likely due to the interaction of the slots with the traveling wave generated in the horizontal polarization.

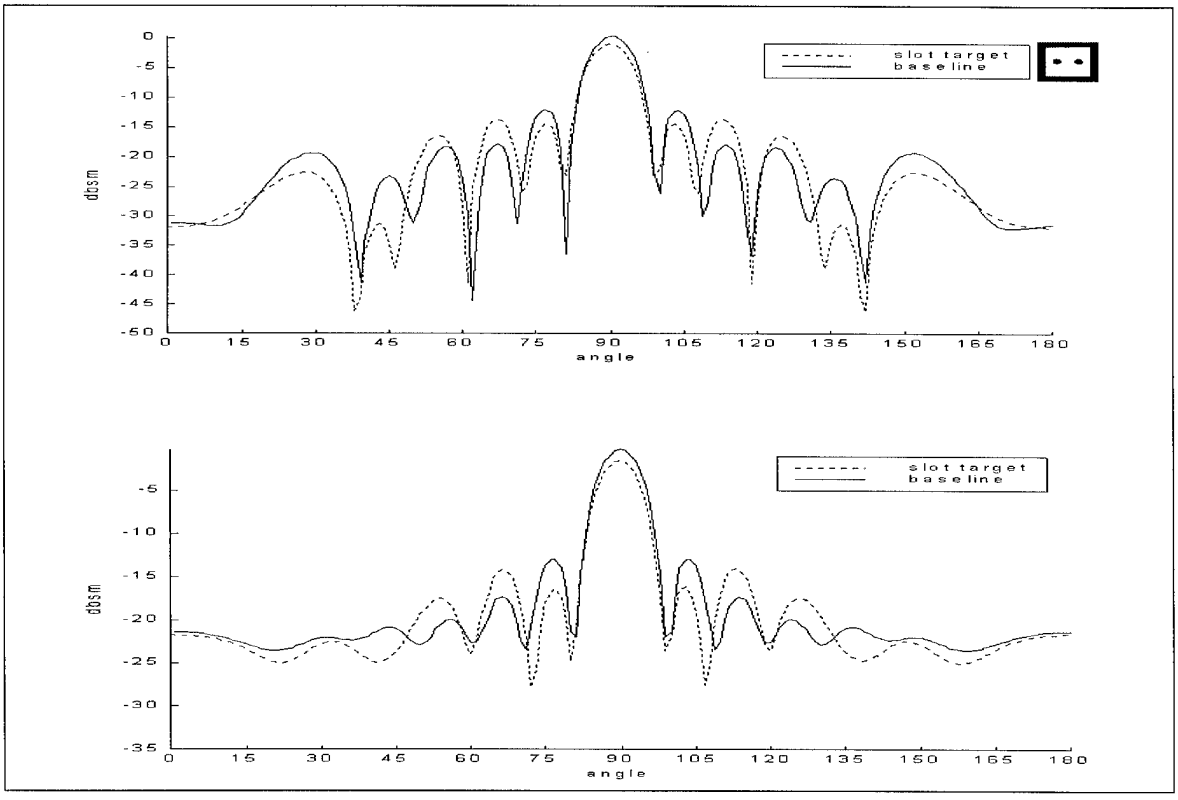

Figure 3. 13: Large 2 circular slots plate (d = 1.5λ) at 10.04 GHz top: Hpol bottom: Vpol

For completeness the enhanced regions are compared with the monostatic array factor for the target at the incident frequency (Figure 3.14). What is particularly interesting in the comparison is the lobe at 67^{o} . The lobe is significantly enhanced in both polarizations while the array factor there is near a negative maximum. In all the previous examples there was definite correspondence between the sign of the array factor and whether the region was enhanced. This latter case clearly shows that relative phasing rather than signed magnitude of the array factor is truly the important consideration for enhanced regions. That is, both positive and negative lobes of the array factor have the potential to enhance radar cross section depending on its phase relation to the structural term. In fact the relative phase of the array and structural term is the fundamental parameter used for the coherent summing of the fields in the analytic expression of Equation (1-1). The analytic solution of the slotted plate is plotted against the measured results for the vertical polarization in Figure 3.16.

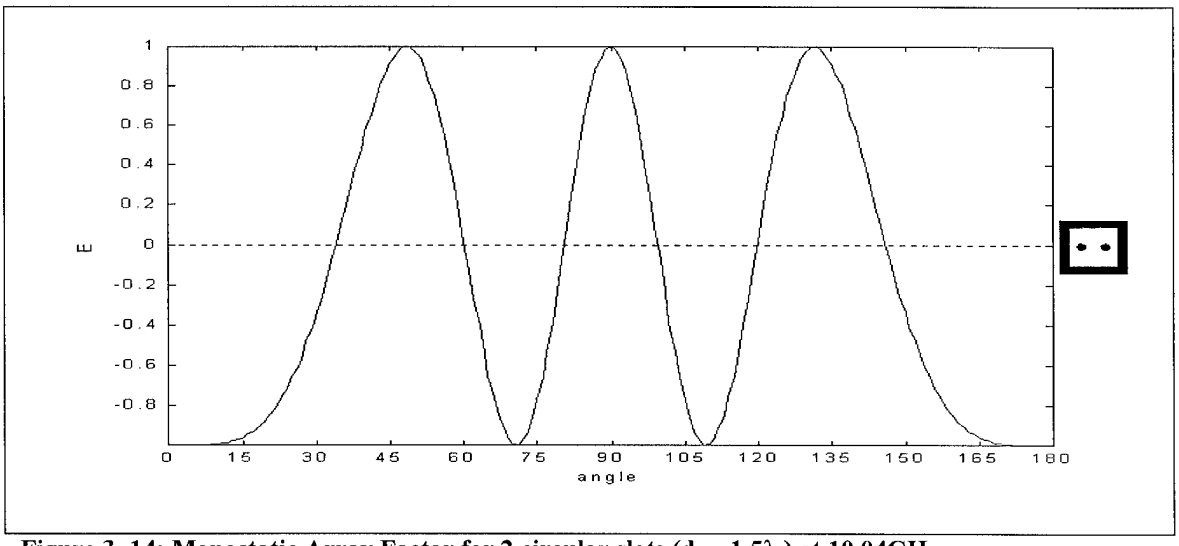

Figure 3. 14: Monostatic Array Factor for 2 circular slots (d = 1.5λ) at 10.04GHz

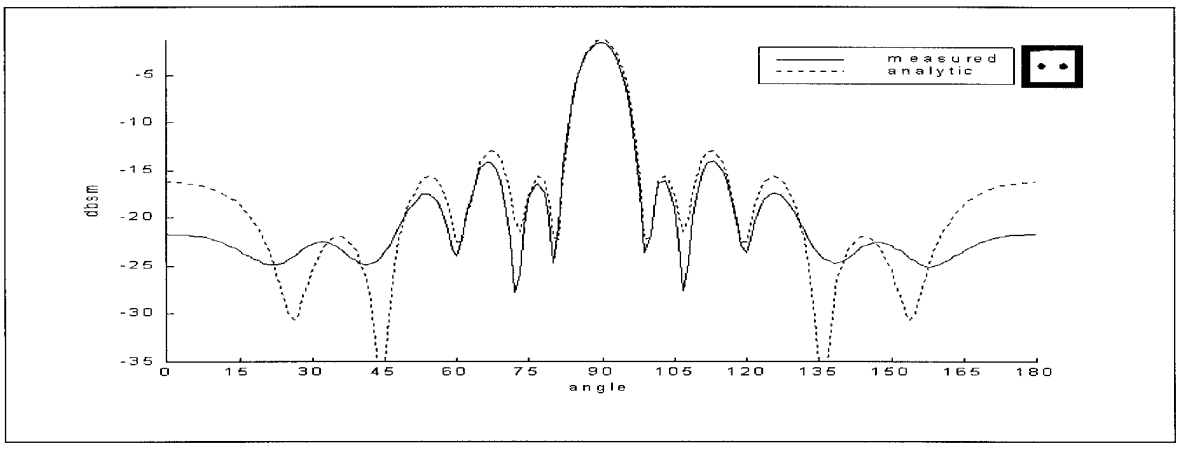

Figure 3. 15: Analytic vs. Measured RCS for Large Plate 2 Circular Slots (d=1.5λ) at 10.04GHz Vpol

For some of the cases of flat plates above it is noticed that there is some reduction of RCS at the broadside incidence for measured targets compared to the baseline; for example, Figure 3.13. This reduction was the intended effect when Green [3] and other researchers did much of the pioneering work on impedance loading. A short answer to why the cross section is reduced is to realize that the open slot presents a reactive load to the incident field. Reactive implies energy storage in the steady state. Thus, not all of the incident energy gets reradiated as we might expect for the PEC surface and PEC equivalent surface of the aperture. Reactance, of course, is a frequency dependent phenomena, the reduction is typically only over small bandwidths (this is why most low observable platforms currently incorporate material absorbers).

Numerical results for linear arrays of circular slots were also computed. The poor convergence to measured values near grazing incidences in the vertical polarization is again evident in the circular slots, although the general trends are picked up. However, accuracy is reasonable from 40^{o} to broadside. Results are somewhat better in the horizontal polarization except that the last null in the RCS pattern is not picked up. The

numerical results are again mesh converged. Similar trends occurred for other circular slot array configurations in both the large and small plates.

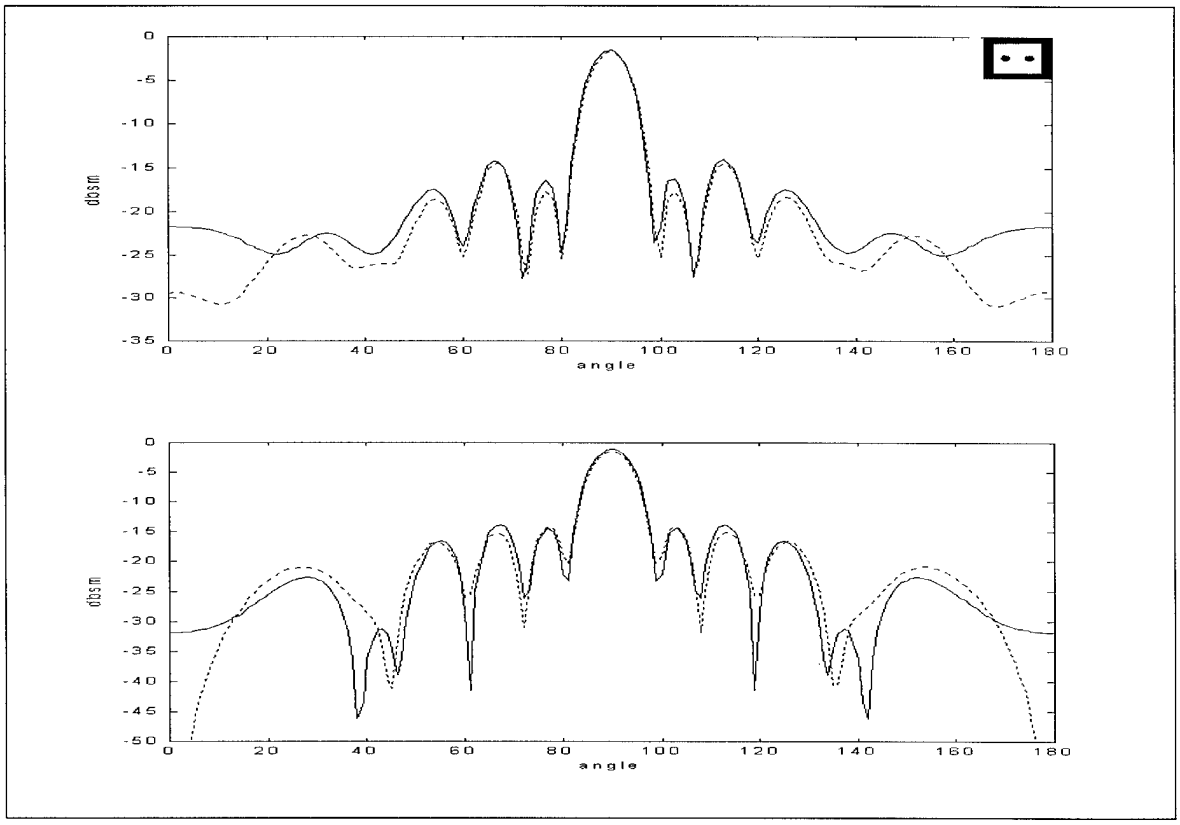

Figure 3.16: Top: MoM prediction of large 2circular slot plate at 10.04GHz Vpol Bottom: Same target Hpol. Dashed lines represent MoM solution and solid lines represent measured target data.

It has been shown how a linear array of slots can be used to enhance radar cross section of a simple target. By extending from a linear to a planar array even greater levels of enhancement can be achieved. Consider any of the above mentioned target configurations. Referring to the target coordinate system given in Chapter 2, the array can be described as having N elements in the x direction. Now for each of those elements space M copies of it in the z direction. Equation (1-1) can be rewritten in terms of N and M as:

$$E_{tot}^{s} = \left[\frac{\sin(Nkd_x \sin\theta\cos\phi)}{N\sin(kd_x \sin\theta\cos\phi)} \times \frac{\sin(Mkd_z \cos\theta)}{M\sin(kd_z \cos\theta)} \right] NME_{element}^{s} \quad (3\text{-}2)$$

The first term in the brackets is recognized as the monostatic array factor in the x direction For elevations near the $\theta = 90°$ plane the second term in the brackets (z directed monostatic array factor) will approach unity. In effect, the array factor for x is simply multiplied by a factor of M. In the more general case, the planar array spacing can be used to control RCS enhancement for both azimuth and elevation radar cross section cuts.

Two cases of the planar array are explored; the first is a large plate 2x2 circular slot array where the spacing is $d_x=d_z=1.5\lambda$ (Figure 3.18). The second case is a 2x3 circular slot array where $d_x=1.5\lambda$ and $d_z=.75\lambda$ (Figure3.19). As stated above, for the $\theta = 90°$ scan plane the planar array just adds a multiplicitive factor M to the linear array factor in x. Theoretically, the target RCS for the four or six slotted plate should demonstrate the same phenomenology as the linear analog, only more pronounced as the slot number goes up.

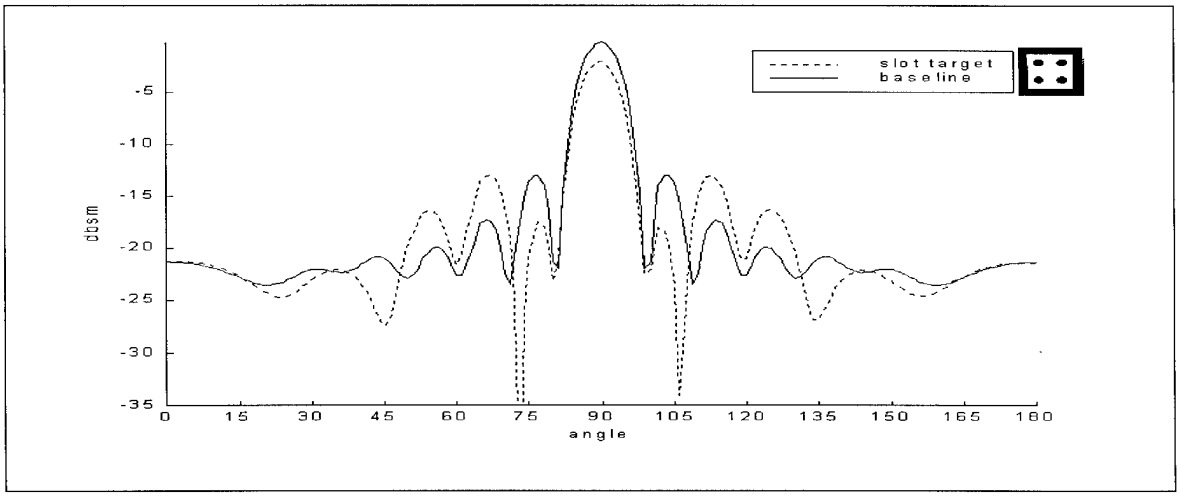

Figure 3. 17: 2x2 circular slot array for large plate at 10.04GHz Vpol.

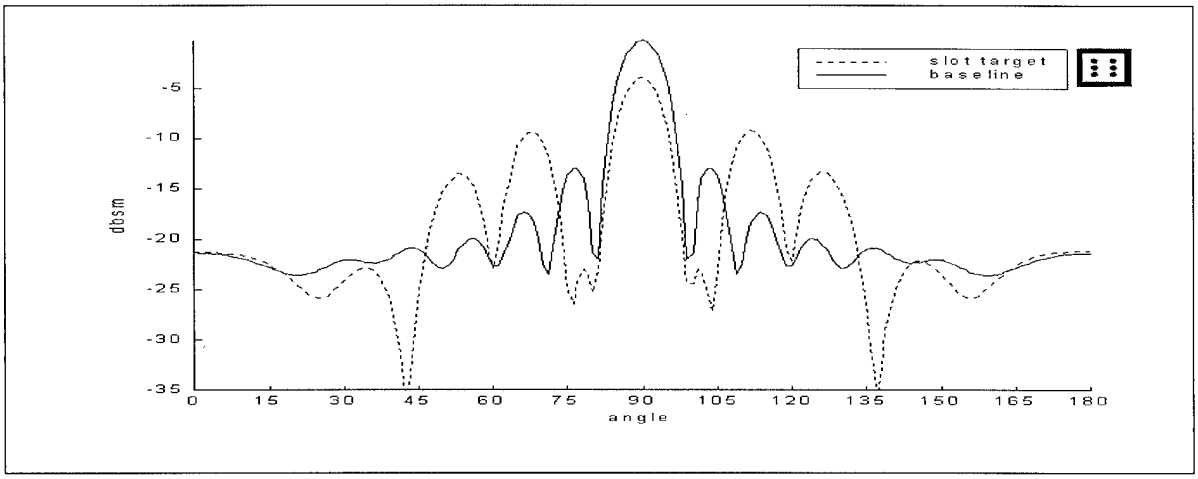

Figure 3. 18: 2x3 circular slot array for large plate at 10.04GHz Vpol

Next, the analytical formulation is applied for a planar array configuration. The results, in general, are still reasonable outside of grazing incidences in that they follow the general trend of measured RCS in most cases, but start to break down as element-edge coupling increases with the element number. Also, discontinuity scatterers can exist for both polarizations with circular slots. These discontinuity scatterers increase as slot number increases, and contribute scattered field components that can significantly alter the RCS. Neither edge coupling nor discontinuity scattering is treated in the analytical expression so as these effects become more significant the errors in predicted RCS accumulate. In most cases, though, the errors are generally less than 4dB at sidelobe peaks not including reactive energy storage near broadside. The only exceptions to this are the six element plates for the vertical polarization. The first sidelobe exhibits errors around 6dB. Also, in the larger arrays (six and nine element) the approximation tends to widen the far sidelobes in the horizontal polarization. Examples of these types of effects are demonstrated in the large plate 2x3 circular slot array configuration in Figure 3.19 below. Again similar trends are exhibited for the smaller targets measured as well.

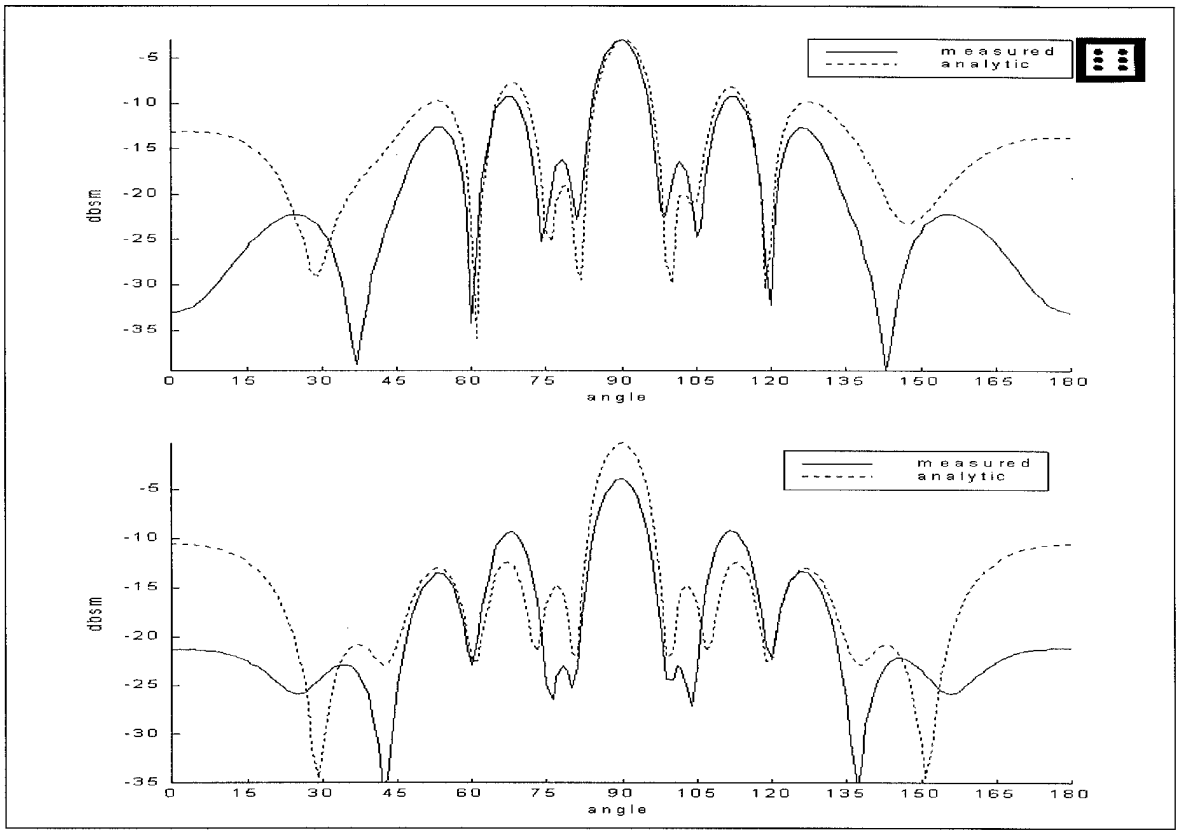

Figure 3. 19: Analytical approximation vs. measured results for large plate with 2x3 circular slot array: Top: Hpol Bottom: Vpol

Finally, enhancement bandwidth limitations for slotted flat plates is considered. Enhancement bandwidth is defined as the range of frequencies for which the radar cross section of the modified target exceeds that of the baseline. Two factors primarily determine bandwidth. The first is the strength of the radiated field and its radiation pattern. In other words, the stronger the field and the wider the lobe the larger the bandwidth. The more dominating influence though is array's response. Once the lobe peaks of the array move away from the region of interest, or a null moves in, very little enhancement, if any, will occur. Figure 3.20 plots the frequency response and array factor for the large plate three slot target with λ separated slots for the horizontal polarization for the enhanced peak at 56^{o} (See also Figures 3.1,3.3,3.5).

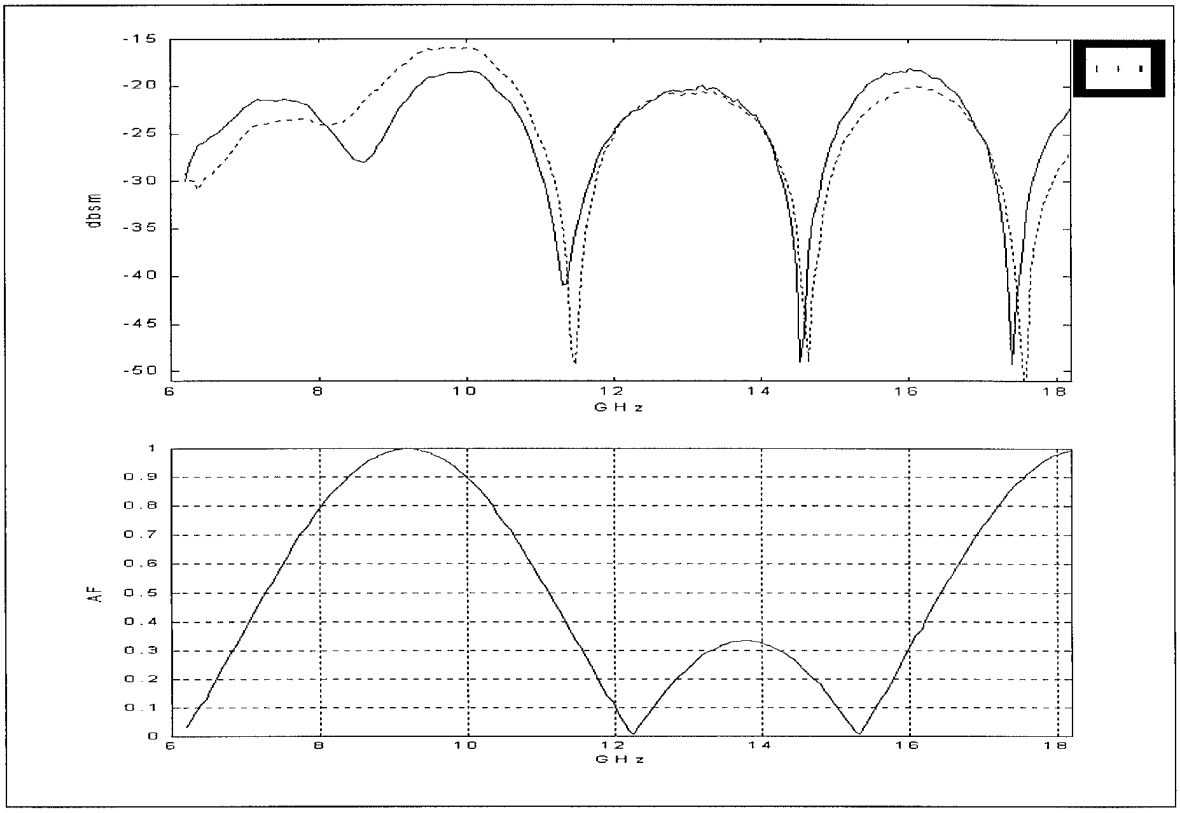

Figure 3. 20: Top: RCS of large 3 slot plate at 56°. The dashed line represents the slotted target and the solid line represents unslotted (baseline) target. Bottom: Associated array factor magnitude

3.3: Cavity Backed Plates

The RCS of a target can be enhanced even further by using cavities to redirect forward-scattered energy into the backscatter direction. The cavity backing concept in the first order sense is very similar to the feeding of a waveguide, that is, by spacing the feed probe one quarter wavelength from the waveguide back wall the reflected wave adds in phase with the wave generated at the feed and field strength is effectively doubled. The cavity backing can be essentially modeled as the backend of the waveguide where the aperture is the feed. The forward scatter fields of the slots are projected into the waveguide. Because of the phase taper across the front face the beam from the array will be steered into the cavity at an angle equal to the incidence angle of the original field.

The normal projection of that field is what travels through and interacts with the guide. The normal projection (k_x) can be recast as a 'projected frequency' inside the cavity. The projected frequency being the frequency in the guide for which the normal wavenumber component corresponds to. Additional enhancement will occur where the total electric path length for the projected frequency is an integer multiple of 2π, that is, where the cavity depth is odd multiples of $\lambda_g/4$. So the cavity depth should be chosen such that it is an odd multiple of $\lambda_g/4$ for the normally projected frequency component at the region of interest.

If the total cross section of the slots is small compared to the cross section of the cavity backing then a resonant cavity model also seems to work well. This is because there is less perturbation due to the boundary condition enforcement on the front face. If the projected frequency component happens to fall in a resonant mode along the cavity depth the reflected wave will come back in phase and additional enhancement will occur.

The level of enhancement is difficult to predict for a cavity-backed structure regardless of whether a waveguide or resonant cavity model is used. This is because it is no simple task to determine how much of the incident power is coupled into the existent modes in the structure. Some intuitive assumptions can be made though. The maximum enhancement realizable is +6dB. This assumes all of the energy in the cavity is coupled into a single mode and is reflected back in phase with the field at the array. The field is doubled and thus corresponds to 6dB gain. The second assumption is that enhancement levels are higher for shallower and narrower cavities. Under these conditions fewer modes exist for a given frequency and thus it is likely that more power is available in modes that do contribute to RCS enhancement.

Before analyzing cavity-backed plate data some caution needs to be exercised before drawing any conclusions about enhancement. The major factor that must be considered is how big the scattering contributions and interactions of the external sidewalls are for a given aspect. In a high frequency sense plate scattering is essentially diffraction from the edges. The cavity sidewall essentially adds another plate at a right angle to the front face, which means at least three edges must now be considered. (Figure3.21)

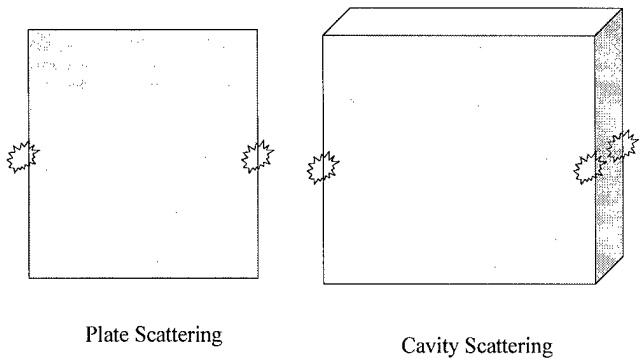

Figure 3. 21: Plate vs. Cavity scattering centers

The baseline structure therefore must be a cavity box, which is essentially a flat plate with the same cross sectional area and depth of the cavity. This structure will incorporate the sidewall effects so an "apples to apples" comparison can be made. The hypothesis is again made that the differences in RCS are due mainly to the influence of the array; furthermore, the array itself is influenced by the cavity parameters which determine the phase progression of the reflected field back to the apertures and thus affect the over all magnitude of enhancement.

Cavity analysis starts with the large 3 rectangular slot with λ spacing for the horizontal polarization at 10.04 GHz. Figure 3.22 shows the RCS plotted against the cavity box and the monostatic array factor below. To verify that the effects are primarily influenced by the array a background subtraction was attempted (Figure 3.23).

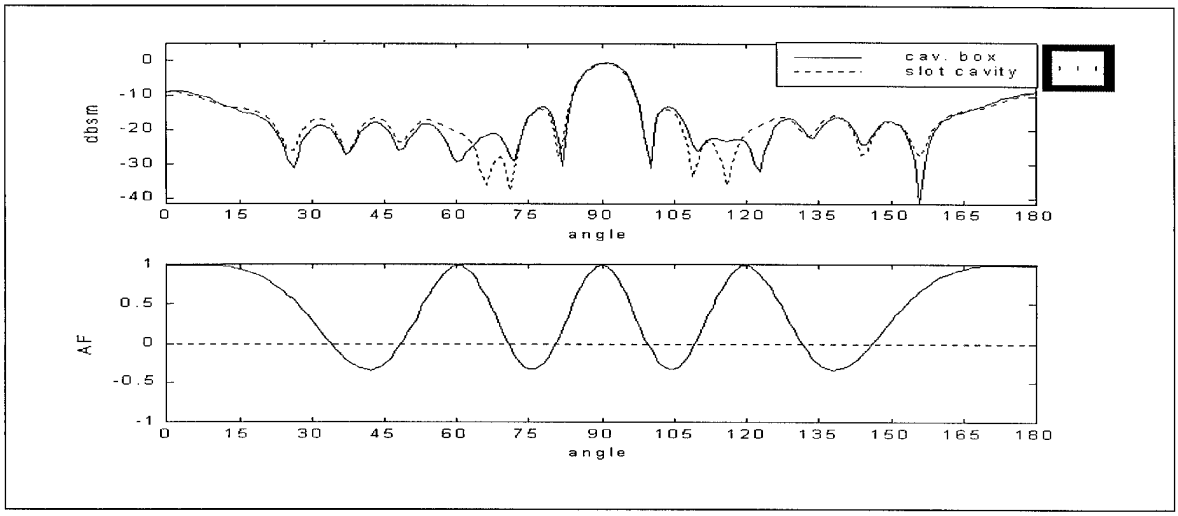

Figure 3. 22: Large 3 slot (d = λ) cavity backed plate at 10.04GHz Hpol.

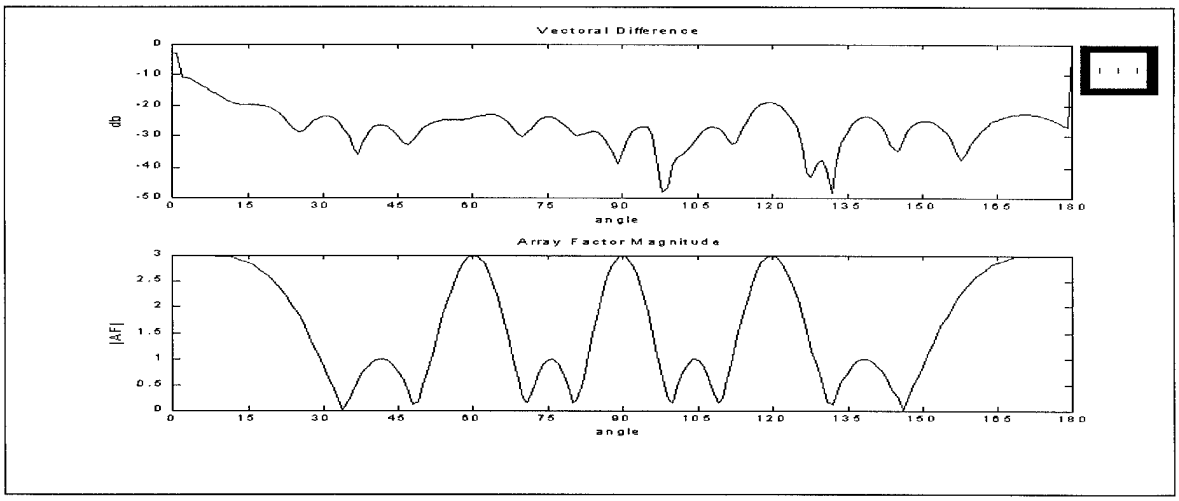

Figure 3. 23: Background subtraction of the 3 slot cavity backed plate in Figure 3.22

The results of the background subtractions are generally poor; however, comparison with the array factor shows excellent correspondence of the difference nulls with the array factor nulls. Also, there is good correspondence between the

distinguishable lobe peaks in the difference plot and the array factor (e.g. 40°, 75°, 120°, and 140°). This gives some merit to the hypothesis that the array factor influences most of the change in RCS compared to baseline targets.

For the target of Figure 3.22 the resonant cavity approach is applied, that is, the resonant modes of the cavity determine which projected frequencies are reflected back in phase, further enhancing target RCS. It is observed that minor enhancements occur at 31°, 40°, and 56°. Also, there may be reduction at 67° . The later is difficult to verify with certainty due to the asymmetries in the target measurement at that angle. The projected frequencies of the enhanced peaks are approximately 5.17GHz, 6.45GHz, and 8.32GHz. The nearest depth resonant modes are 5.27GHz, 6.24GHz, and 8.33GHz. Because of the weak array factor magnitudes at 31° and 40° not much enhancement would be anticipated; furthermore, the projected frequencies are not very near any resonant modes therefore there is little constructive interference from the cavity to compensate for the low array factor in these regions. The projected frequency at the 56° lobe peak is very near a resonant mode; however, it is the ninth resonant mode in the depth dimension. Much of the energy is likely consumed in the excitation of other modes that do not necessarily contribute to enhancement. This in turn reduces the over all level of enhancement at that aspect.

For the vertical polarization rectangularly slotted cavities appear much like the cavity box baseline due to cutoff effects of the apertures. An RCS plot for the five slot case is shown in Figure 3.24. (Data is not available for the three slot case of Figure 3.22, but the effect is intuitively the same).

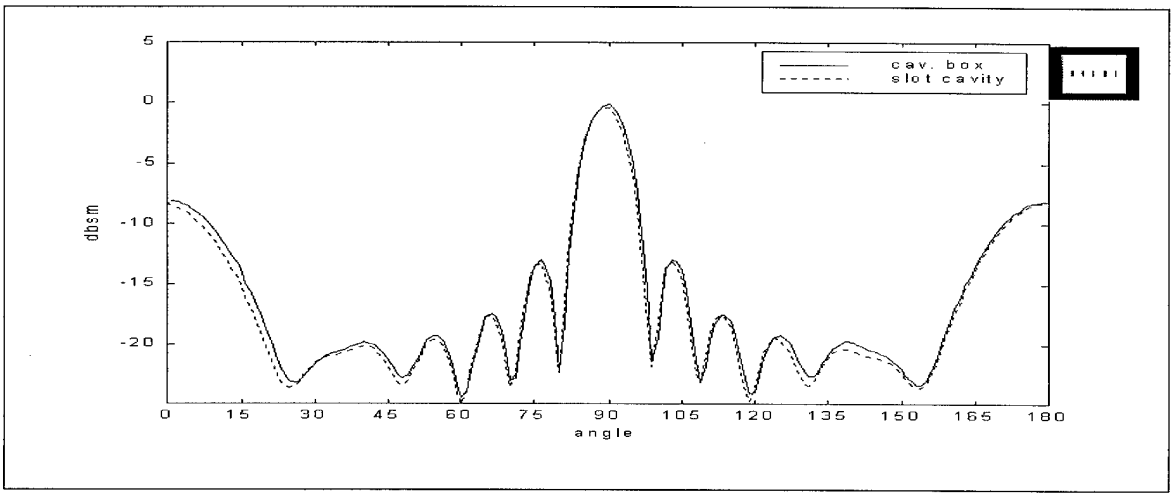

Figure 3. 24: Five rectangular slot cavity Vpol at 10.04GHz

Analysis is now shifted to the circular slotted plates. The first case examined is the large 3x1 circular slot array (d_x=.75λ) illuminated at 10.04GHz. A background subtraction is applied to verify RCS changes are influenced primarily by the array. A plot of the vector subtraction for the horizontal polarization is shown in Figure 3.25 and the target RCS is plotted in Figure 3.26 for both polarizations.

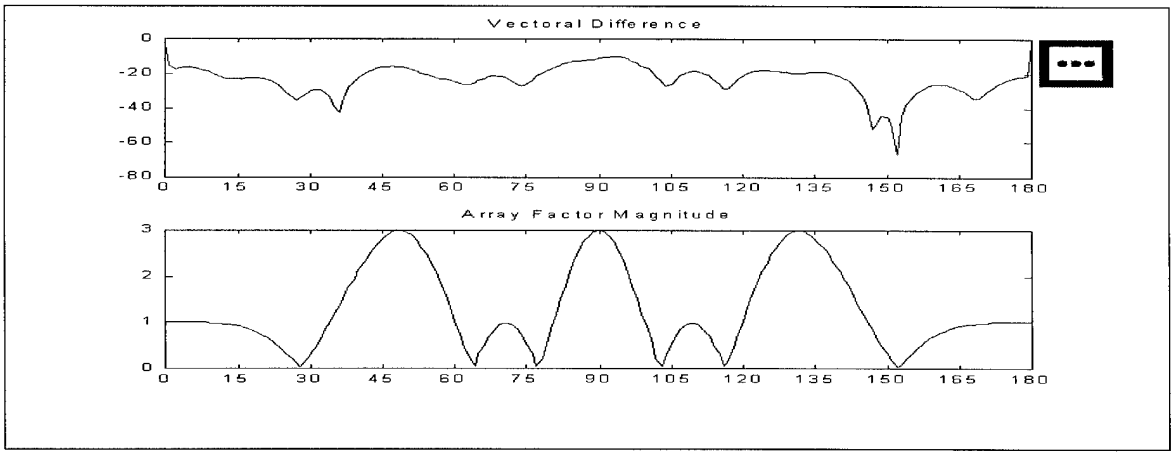

Figure 3. 25: Background subtraction for large cavity backed 3x1 circular slot array for 10.04GHz Hpol

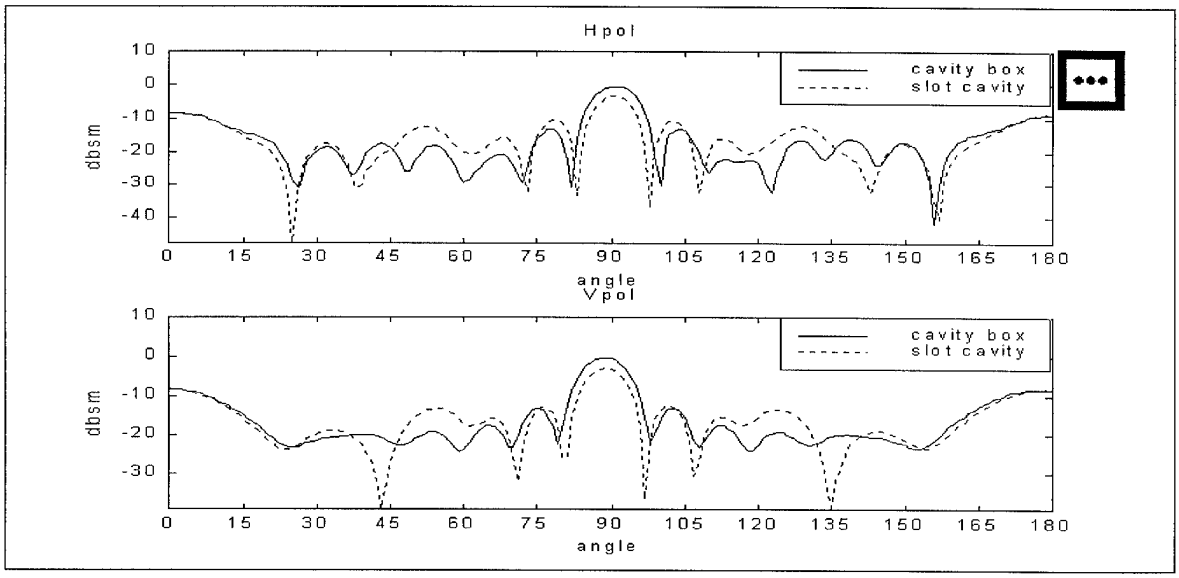

Figure 3. 26: RCS of large cavity backed circular slot array for both principle polarizations at 10.04GHz

The structure was also analyzed using a resonant cavity approach. There were two regions primarily enhanced, the lobe peaks at 55° and 66°. Also, for the horizontal polarization there was slight enhancement at the 77° lobe peak. The projected frequencies at these aspects are 8.22GHz, 9.17GHZ and 9.78GHz respectively .The nearest corresponding resonant modes are at 8.33GHz, 8.98GHz, and 9.72GHz respectively. The mode sequence (order in which modes appear), proximity to a resonant mode, and array factor strength (Figure 3.25) are all consistent with the enhancement levels observed for the target in the horizontal polarization. The levels appear somewhat lower in the vertical polarization. This can be explained by the *cos(ϕ)* element factor term that appears in the radiated field expression for the circular slot for the vertical polarization. [Refer to Equations (2-3) and (2-4)].

Next the plate in the above example is extended from a 3x1 to a 3x3 array. The spacings are equivalent in the x and z directions ($d_x=d_z=.75\lambda$). This example is good in

demonstrating why in a first order sense it is difficult to predict cavity response. In this case the same regions are affected however the enhancement levels are much stronger for the lobe peaks at 66^{o} and 77^{o} (Figure3.27). It is likely that due to the presence of apertures over a greater area of the front face allows certain modes that were not able to contribute in the linear array to contribute in the planar case. The additional contribution then adds to the total enhancement effect. The same phenomena was observed with a 2x1 (dx=.1.5λ) and 2x3 (dx=1.5λ, dz=.75λ) cavity backed circular slot plate.

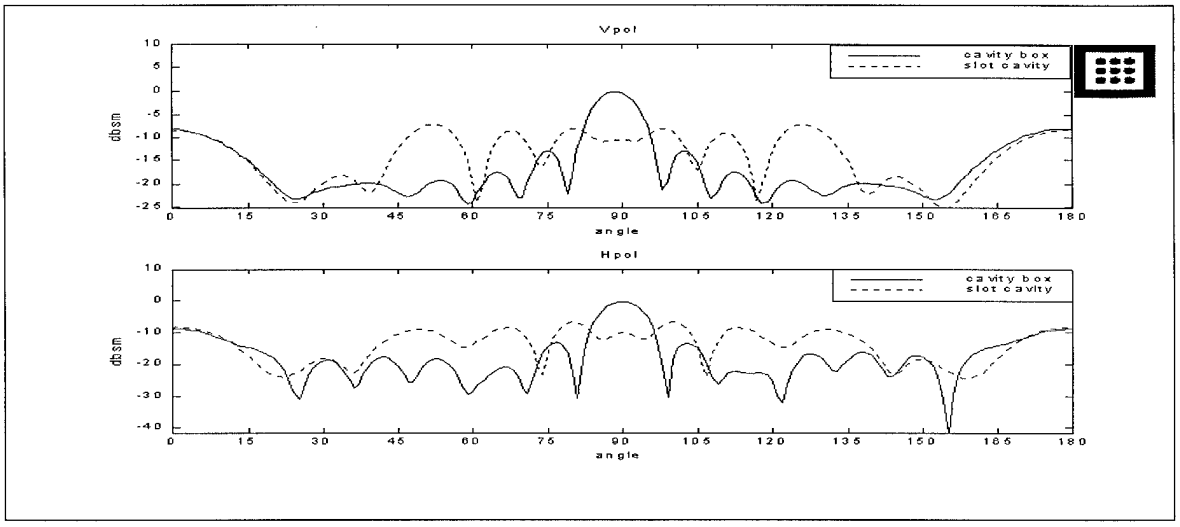

Figure 3. 27: Large cavity backed 3x3 circular slot array for both principle polarizations at 10.04GHz

Next, comparisons are made between measured results and the moment method predictions computed by FISC. Unfortunately the moment method predictions were not very consistent with measured results. This can be explained in the way the integral equation is developed and how the facet file was generated. FISC uses the combined field integral equation (CFIE) as a default to solve for the scattering of closed surfaces. The MFIE component wants to see two surface normals to compute the currents of the discontinuous magnetic field. The facet file was generated assuming infinitely thin faces (surface shell mesh) patched together at the edges. The shells will only report one surface

normal, the outer normal, in the facet file. Thus the code never sees the interior of the cavity and solves the solution of essentially the cavity box perturbed by the slots of the front cavity face. Figure 3.28 shows an example of this for the large cavity backed 2x3 circular slot array. The cavity problem could be better solved by either incorporating a thickness into the facet file creating the two surface normals necessary or by using some other CEM technique that directly solves for the fields in a spatial grid, for example the Finite Difference Time Domain (FDTD) method.

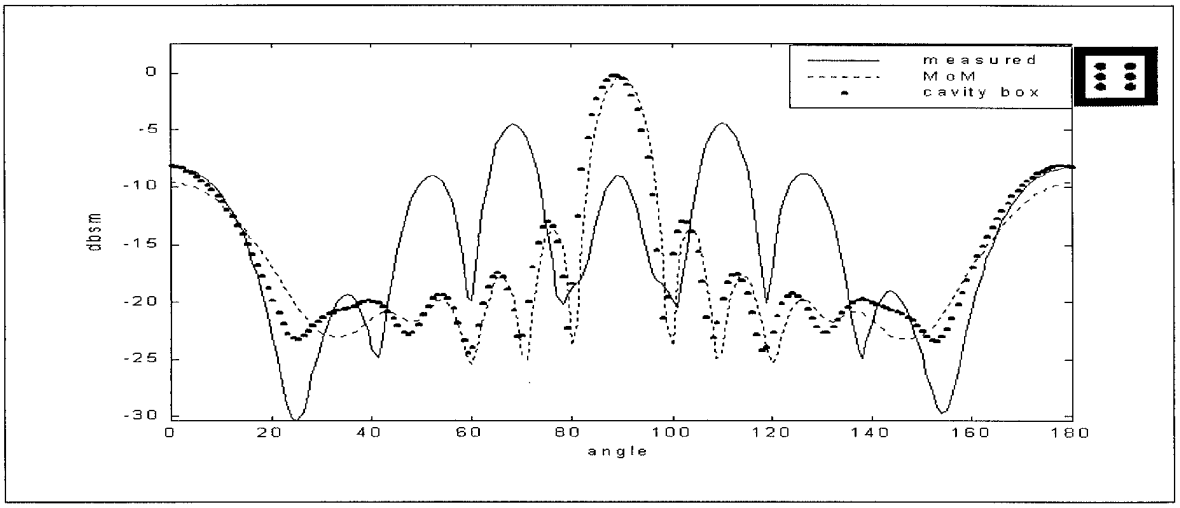

Figure 3. 28: MoM solution vs. measured and cavity box RCS for large plate 2x3 circular slot array 10.04GHz Vpol. The target facet file assumes infinitely thin faces, thus generating only one surface normal for the CFIE. This in turn makes the inside of the cavity invisible.

Finally, bandwidths of enhanced regions are examined. One of the key factors for cavity backed plates much like the flat plates is the array response as a function of frequency. However, as might be suspected the cavity parameters play a significant role as well. The modal configuration changes as well as the electrical depth of the cavity, this allows for possible jumps and dips in RCS depending on whether the incident wave is in a resonant mode or the electrical path length is in or out of phase. Typically, though, the

bandwidth for the cavity backed structure is narrower in the design frequency region but the enhancement level is higher. Also, there are additional jumps in RCS outside the bandwidth of the plate alone due to resonance effects of the cavity structure. Figure 3.24 below shows two different cases of plate and cavity backed plate structures. The first is for a 2x1 array of circular slots on the large plate at 67^{o}. The second is for a 3x1 array of circular slots at the same incidence. Note that the unnormalized array factor peak at that incidence for the former configuration is near –2 at 10GHz and the latter is about –1.2.

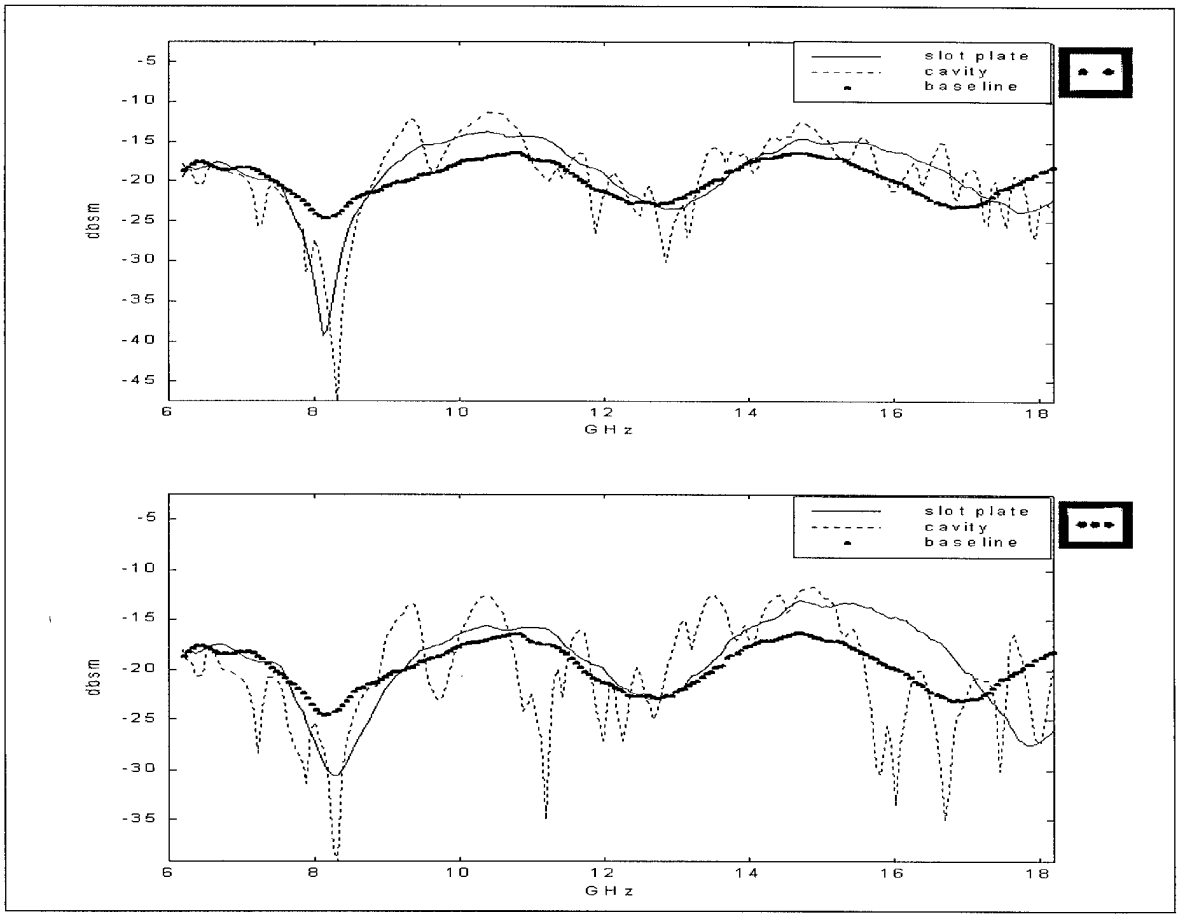

Figure 3. 29: Bandwidth plot of large cavity and plate for 2x1 and 3x1 circular slot array.

3. 4: Sphere and Ogive

The sphere and ogive measurements were taken primarily to get some general insight into the RCS enhancement effects when these structures are slotted. These geometries behave similar to the plates with respect to the influences of the slot arrays and cavity effects. There is one major feature evident in the curved geometries though not present in the flat targets; the ability of the cavity and array to enhance the broadside RCS.

Cavity backings behind flat surfaces are unable to enhance at broadside. This is because the strongest return from a flat specular flash is the totally reflected power over the cross section of the target. Total reflection assumes an entirely open or shorted geometry, that is, the broadside RCS of flat plate or equivalent aperture. In other words the target cannot reflect more power than it is able to intercept (conservation of energy).

In the case of curved geometries, however, there is a spreading factor associated with a specular reflection, thus not all of the power intercepted by the target at specular incidence can be recaptured. The slot structure in this case can be employed to refocus some of that energy in the specular direction, creating an enhanced RCS at that aspect. The enhancement can be augmented further by the appropriate choice of cavity parameters. However, as stated earlier, cavity parameters for the sphere and ogive targets are much more complicated to calculate and control.

Plots of the small sphere and ogive targets are provided in Figure 3.30 and Figure 3.31 below. Sphere data is compared to exact results of the Mie Series solution and ogive data is compared to measurements of an unslotted ogive target. Both frequency sweep

and pattern cut measurements are shown. Frequency sweeps are taken at the broadside aspect and pattern cuts are taken at the fundamental resonance of the slots.

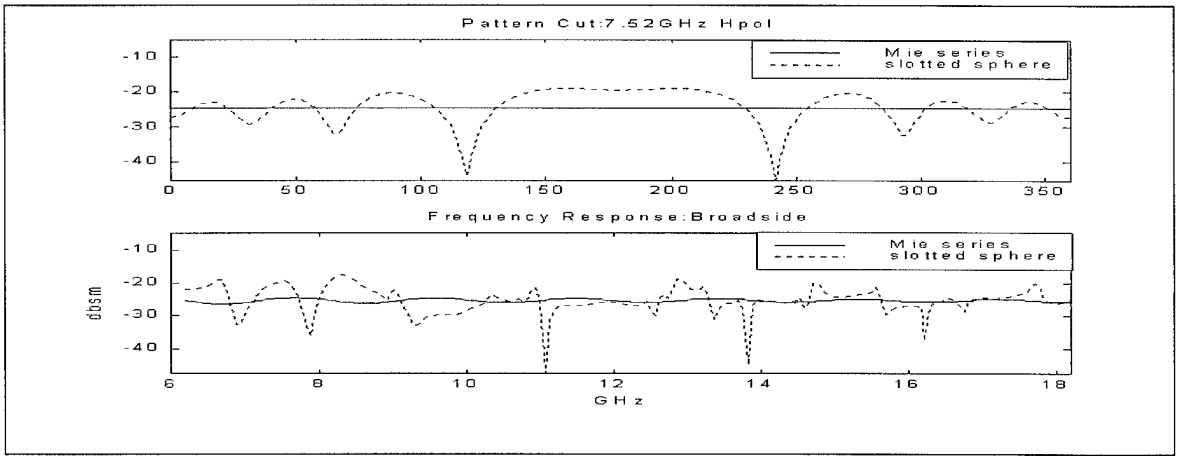

Figure 3. 30: Pattern cut and frequency sweep for small slotted sphere

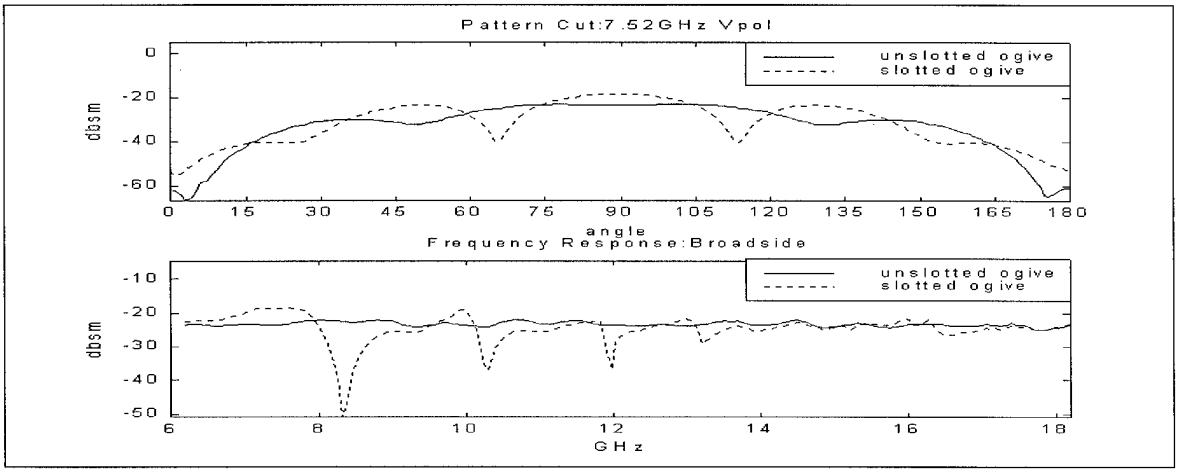

Figure 3. 31: Pattern cut and frequency sweep for small slotted ogive

CHAPTER 4: CONCLUSIONS

A technique of using periodic open slots to passively enhance radar cross section was explored. The bulk of the research effort was taking actual RCS data measurements of simple slotted targets. The target sets were modified with various slot numbers, sizes, spacings, and geometries. The targets were compared against unmodified baseline targets as well as against targets with different slot configurations. Several first order principles about arrays and apertures were experimentally verified.

Second, computer predictions using FISC, a method of moments code were run for the target set. It was found that the moment method worked reasonably well for the flat plate targets but failed to capture the effects of cavity geometries due because of the way the targets were modeled. Better computational results might be achieved using other CEM techniques or modeling the target geometries with finitely thick faces in order to generate the two surface normals required by the MFIE and CFIE

A first order analytical approximation to the scattering by the slots was tested against measured data. The approximation though does not take into account coupling to edges or discontinuity scattering for the horizontal polarization. Results in most cases were reasonably close to the actual measured data for aspects between 25^{o}-90^{o}. The errors accumulate though as slot number and their proximity to the edges increase. The worst case error for the targets tested was about 6dB but was typically within 1dB to no more than 4dB outside of grazing incidence.

Also, a waveguide and resonant cavity approach was investigated in order to attempt to describe which regions a cavity backed structure would further enhance. Cavity analysis was difficult to perform over a broad aspect because of sidewall

contributions interfering with the cavity effects of the front face. Background subtraction was not effective in many cases because of the constant removal and remounting of the target on the range. The misalignments of successive measurements destroy the phase relations required for a good background subtraction. These difficulties might be overcome for future measurements if cavities are mounted in a test body. While it was difficult to estimate the exact level of enhancement it was shown that at least the regions could be predicted.

The true test of the utility of the analytical expression would be to use it from a design perspective rather than an analysis one. If the RCS of a plate or other target could be enhanced to a set criteria using the analytical expression to determine the slot and array parameters, and the performance could be computationally or experimentally verified then engineers would have a fast and powerful tool to use for RCS enhancement applications.

Bibliography

1. Balanis, Constantine A., Advanced Engineering Electromagnetics, New York: John Wiley and Sons Inc, 1989.

2. Balanis, Constantine A, Antenna Theory: Analysis and Design ,2nd ed., New York: John Wiley and Sons, 1997.

3. Green, R. B., "The General Theory of Antenna Scattering," Report 1223-17, Antenna Laboratory, Ohio State University, September 1961.

4. Hansen R.C., "Relationships Between Antennas as Scatterers and Radiators," Proc. IEEE, Vol. 77. May 1989, pp. 659-662

5. Knot, Eugene F. and others, Radar Cross Section, 2nd ed. , Boston: Artech House 1993.

6. Ruck, J.T. and others. Radar Cross Section Handbook, Vol. 2., Plenum Press, New York, NY, 1970

7. Wood, William D. Electromagnetic Scattering from a Cavity in a Ground Plane: Theory and Experiment. PhD Dissertation Air Force Institute of Technology Wright-Patterson AFB OH, Mar 97

REPORT DOCUMENTATION PAGE	Form Approved OMB No. 0704-0188

1. AGENCY USE ONLY *(Leave blank)*	2. REPORT DATE	3. REPORT TYPE AND DATES COVERED
	March 1999	Master's Thesis

4. TITLE AND SUBTITLE
Radar Cross Section Enhancement of Simple Targets

5. FUNDING NUMBERS

6. AUTHOR(S)
Brian J. Crothers, 1Lt, USAF

7. PERFORMING ORGANIZATION NAME(S) AND ADDRESS(ES)
Air Force Institute of Technology
2950 P Street
WPAFB OH 45433-7765

8. PERFORMING ORGANIZATION REPORT NUMBER
AFIT/GE/ENG/99M-06

9. SPONSORING/MONITORING AGENCY NAME(S) AND ADDRESS(ES)
AFRL/XPN
2591 K Street
WPAFB 45433-7602

10. SPONSORING/MONITORING AGENCY REPORT NUMBER

11. SUPPLEMENTARY NOTES
Sponsor Name:Dr William Wood ph# 937-255-0270
Advisor Name: Dr Vittal Pyati,Professor ph# 937-255-3636 x4576 email Vittal.Pyati.afit.af.mil

12a. DISTRIBUTION AVAILABILITY STATEMENT
Approved for public release; distribution Unlimited.

12b. DISTRIBUTION CODE

13. ABSTRACT *(Maximum 200 words)*

The purpose of this research was to explore the use of periodic open slots on simple target geometries as a passive antenna array to selectively enhance radar cross section.The structures were then backed bya shallow cavity in an attempt to further enhance the radar cross section. Moment method predictions as well as an analytic expression for antenna scattering were compared with experimental results. It was found that the changes in radar cross section was consistent with the radiated fields of the array. Also cavity backed structures were shown to provide significant additional enhancement at certain incidence angles depending on the cavity dimensions. Moment method solutions generally showed strong agreement, though, special care needs to be taken when modeling cavities. The analtic solution worked well in most cases, however, errors accumulate as the number of elements in close proximity to edges increase.

It was shown that the use of slotted and cavity structures if properly designed could be an effective means of selectively enhancing radar cross section.

14. SUBJECT TERMS	15. NUMBER OF PAGES
radar cross section, enhancement, slot arrays, cavity backed structures,antenna scattering	59
	16. PRICE CODE

17. SECURITY CLASSIFICATION OF REPORT	18. SECURITY CLASSIFICATION OF THIS PAGE	19. SECURITY CLASSIFICATION OF ABSTRACT	20. LIMITATION OF ABSTRACT
UNCLASSIFIED	UNCLASSIFIED	UNCLASSIFIED	UL